Signalling speed along a key white matter tract influences memory recall ability in humans

Ian A. Clark[1], Siawoosh Mohammadi[2], Martina F. Callaghan[1] & Eleanor A. Maguire[1*]

[1]Wellcome Centre for Human Neuroimaging, Department of Imaging Neuroscience, UCL Queen Square Institute of Neurology, University College London, London, UK

[2]Institute of Systems Neuroscience, University Medical Centre Hamburg-Eppendorf, Hamburg, Germany

*For correspondence: e.maguire@ucl.ac.uk

Competing interests: The authors declare no competing interests.

Abstract

Conduction velocity is the speed at which electrical signals travel along axons and is a crucial determinant of neural communication. Inferences about conduction velocity can now be made in vivo in humans using magnetic resonance (MR) imaging and a measure called the MR g-ratio. Here, in the first application to cognition, we found that increased MR g-ratio, and by inference faster conduction velocity, specifically in the parahippocampal cingulum bundle, which connects the hippocampus with a range of other brain areas, was associated with better memory recall ability in 217 healthy adults. Moreover, two tract features seemed to favour better memory retrieval – large inner axon diameters and coherently organised neurites, both of which facilitate speedy signalling. These results offer a new perspective on drivers of individual differences in memory recall ability. More broadly, they show that MR g-ratio can provide novel insights into how the human brain processes and integrates information.

Introduction

Communication between neurons in the brain is critical for cognition, and depends upon action potentials being conveyed along axons within white matter tracts. The speed at which these electrical signals travel along axons is known as the conduction velocity. It has been suggested that faster axonal conduction velocity promotes better cognition. For example, an increase in axonal conduction velocity is hypothesised to underpin the greater cognitive processing ability of vertebrates, in particular primates and humans (Brancucci, 2012; Miller, 1994), compared to invertebrates (Arancibia-Cárcamo et al., 2017; Bullock et al., 1984; Nave, 2010). In rats (Aston-Jones et al., 1985) and cats (Xi et al., 1999), faster axonal conduction velocity has been observed in younger compared to older animals. In a similar vein, axonal degradation that can lead to reduced conduction velocity has been identified in older compared to younger monkeys (Peters et al., 2000; Peters and Sethares, 2002). Slower conduction velocity may, therefore, be a factor in age-related cognitive decline.

Echoing these findings from non-humans, estimates of conduction velocity in humans from the latency of visual evoked potentials recorded over primary visual cortex (Reed and Jensen, 1992) and between the thalamus and parietal cortex (Reed and Jensen, 1993) have been positively correlated with nonverbal intelligence quotients. In addition, faster axonal conduction velocities are thought to better explain increases in intelligence than absolute and relative brain volumes (Dicke and Roth, 2016).

That faster conduction velocity might confer an evolutionary cognitive advantage is perhaps unsurprising. The scope for signals to travel quickly and efficiently between brain regions could make all the difference for an individual's survival.

The conduction velocity of an axon is dependent upon two biological features – the axon diameter and the presence and thickness of a myelin sheath (Gasser and Grundfest, 1939;

Hursh, 1939; Huxley and Stämpeli, 1949; Rushton, 1951). A larger axon diameter results in less resistance to the action potential ion flow, resulting in faster conduction velocity. The presence of a myelin sheath around an axon acts like an electrical insulating layer, reducing ion loss and preserving the action potential, and this helps to maintain or even increase conduction velocity. A key factor in determining an axon's conduction velocity is the g-ratio (Chomiak and Hu, 2009; Rushton, 1951; Schmidt and Knösche, 2019), which is computed as the ratio of the inner axon diameter, or radius, relative to that of the axon plus the myelin sheath that encases it (Figure 1A). Given that the g-ratio encompasses information about the inner axon diameter and myelin thickness, differences in g-ratio can help to differentiate which of these two features might be influencing variations in conduction velocity (Caeyenberghs et al., 2016; Kaller et al., 2017; Lakhani et al., 2016; Waxman, 1980; Xin and Chan, 2020). Here we consider four different scenarios, central to our hypothesis testing, from which faster conduction velocity might arise, with each scenario differing in the underlying microstructure and consequently indexed differently by the g-ratio.

In Figure 1F, inner axon diameter, myelin thickness and g-ratio are plotted together. Myelin thickness is represented by the gradient in background colour and contours, with thinnest myelin at the bottom right, and thickest on the top left. The direction of the arrows describes the change in g-ratio for the microstructural variations presented in the four scenarios of interest. Specifically (1) faster conduction velocity could be due to an increase in the thickness of the myelin sheath, with the inner axon diameter remaining constant. This is observed as a decrease in g-ratio values (Figure 1B and Figure 1F, blue arrow). (2) An increase in conduction velocity could arise primarily from an increase in myelin sheath thickness, but one that is also accompanied by a larger inner axon diameter. Here, a decrease in g-ratio would also be observed, but to a lesser extent than when the inner axon diameter remains constant (Figure 1C and Figure 1F, red arrow). (3) Quicker conduction velocity could be due

predominantly to a larger inner axon diameter, but with some increase in myelin thickness also being present. This would result in an increase in the g-ratio (Figure 1D and Figure 1F, orange arrow). (4) Faster conduction velocity could be a consequence of both the inner axon diameter and myelin thickness increasing proportionally to each other, and a constant g-ratio value would be expected in this circumstance (Figure 1E and Figure 1F, black arrow).

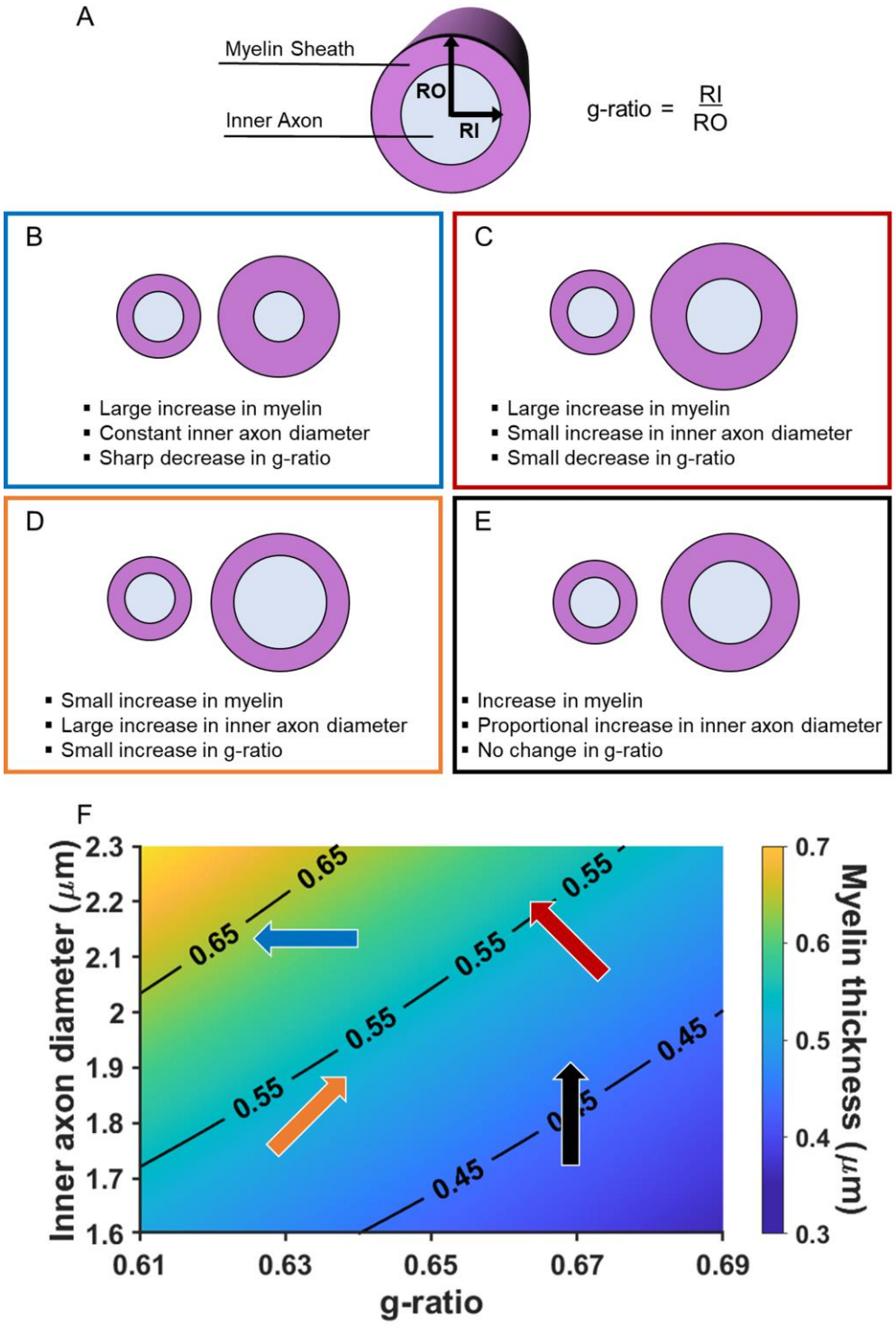

Figure 1. Illustration of the g-ratio and how it relates to specific microstructural properties that could give rise to faster conduction velocity. **(A)** Schematic of a myelinated axon. **(B-E)** Illustrations of how changes in axonal microstructure could result in faster conduction velocity, and how these are manifested in the g-ratio. **(F)** Graphical representation of B-E (see Appendix 1 for details of the simulation). Myelin thickness is represented by the gradient in background colour and contours on the graph, with the thinnest myelin at the bottom right and thickest at the top left. The direction of the arrows describes the change in g-ratio for each microstructural variation presented in B-E. The positioning and colours of the arrows correspond to the text box outline colours in B-E.

Until recently, g-ratio measurements have been restricted to invasive studies in animals, consequently limiting its application. However, by combining diffusion magnetic resonance imaging (MRI) with quantitative structural MRI scans optimised to measure myelination (e.g. magnetisation transfer saturation; Weiskopf et al., 2013), it is now possible to estimate the g-ratio in vivo in healthy humans across the whole brain (Drakesmith et al., 2019; Mohammadi et al., 2015; Mohammadi and Callaghan, 2020; Stikov et al., 2015). This is achieved by measuring an aggregate g-ratio, calculating the ensemble average across a voxel of an underlying microstructural distribution of g-ratios (Stikov et al., 2015; West et al., 2016). Whole brain MR g-ratio maps enable the investigation of the MR g-ratio of white matter fibre pathways at the group level. These MR g-ratio estimates have been optimised (Ellerbrock and Mohammadi, 2018; Jung et al., 2018; West et al., 2018) and used to investigate white matter development (Cercignani et al., 2017), changes in the g-ratio during aging (Berman et al., 2018), and as a potential neuroimaging marker in patients with multiple sclerosis (Yu et al., 2019). As far as we are aware, the MR g-ratio has never been examined in relation to cognition. This is despite the novel insights it could provide, for example, into individual differences.

The rich recall of personal past experiences known as autobiographical memories is a critical cognitive function that serves to sustain our sense of self, enable independent living, and prolong survival (Tulving, 2002). While some healthy individuals can recollect decades-old autobiographical memories with great richness and clarity, others struggle to recall what they did last weekend (LePort et al., 2012; Palombo et al., 2015). In the context of the healthy population, we currently lack a clear biological explanation for the basis of these individual differences (Palombo et al., 2018). There is no doubt that the hippocampus is central to the processing of autobiographical memories, and hippocampal damage is linked with autobiographical memory impairments (McCormick et al., 2018; Scoville and Milner, 1957; Winocur and Moscovitch, 2011). However, no consistent relationship between

autobiographical memory recall ability and hippocampal grey matter volume or microstructure has been identified in healthy individuals (Clark et al., 2020; Clark et al., 2021a; LePort et al., 2012; Maguire et al., 2003; Van Petten, 2004). The hippocampus does not act alone, and functional neuroimaging studies have revealed that a distributed set of brain areas supports autobiographical memory recall along with the hippocampus, including the parahippocampal, retrosplenial, parietal and medial prefrontal cortices (Andrews-Hanna et al., 2014; Maguire, 2001; Spreng et al., 2009; Svoboda et al., 2006). Changes in MR g-ratio and, by inference, conduction velocity, might affect communication between these brain regions and so influence individual differences in autobiographical memory recall within the healthy population.

Three white matter pathways in particular enable communication with the hippocampal region – the fornix, the uncinate fasciculus and the parahippocampal cingulum bundle. The fornix (Figure 2A) is a major pathway in and out of the hippocampus and connects it to the orbital and medial prefrontal cortices, the basal forebrain, the anterior thalamus, the hypothalamus and the mammillary bodies (Aggleton et al., 2015; Croxson et al., 2005). The uncinate fasciculus (Figure 2B) originates in the uncus, entorhinal and parahippocampal cortices and passes over the lateral nucleus of the amygdala, arcs around the Sylvian fissure, terminating in various locations throughout the prefrontal cortex (Croxson et al., 2005; Von Der Heide et al., 2013). The parahippocampal cingulum bundle (Figure 2C) links the hippocampus with the entorhinal, parahippocampal, retrosplenial and parietal cortices, as well as providing another route between the hippocampus and anterior thalamus (Bubb et al., 2018; Jones et al., 2013b). It also links to the prefrontal cortex via its connections with other parts of the cingulum bundle.

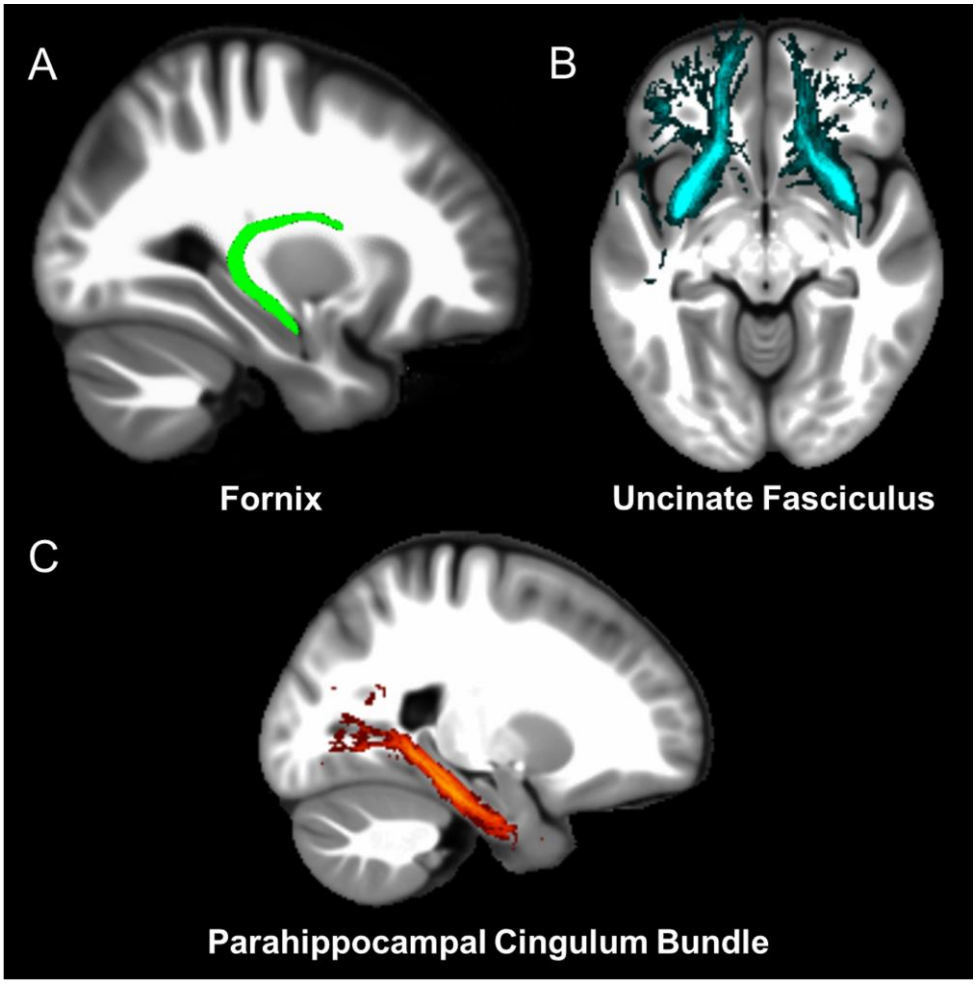

Figure 2. The three white matter tracts of interest, given their relationship with the hippocampal region. The white matter tracts were defined using the Johns Hopkins probabilistic white matter tractography atlas (Hua et al., 2008). with the minimum probability threshold set to 25%, with the exception of the fornix as the available fornix tract was not probabilistic.

In the current study we calculated the MR g-ratio within these three pathways to ascertain whether this was significantly related to autobiographical memory recall ability. The relationship of g-ratio to the underlying microstructure as outlined in Figure 1, allowed us to further gauge whether any significant effects were more likely to be explained by the extent of myelination or the size of the inner axonal diameter of the fibres in these three white matter tracts. As well as the MR g-ratio, we also used the neurite orientation dispersion and density imaging (NODDI; Zhang et al., 2012) biophysical model to derive two complementary

biological measures that could provide further insights into the arrangement of neurites in a voxel. A neurite is any projection from a neuron's cell body, such as an axon or a dendrite. The neurite orientation dispersion index is an estimate of the organisation of the neurites in a voxel, where a small orientation dispersion index value indicates a low dispersion of neurites, in other words, that the neurites are coherently organised. The second property, neurite density, is a measure of the density of the neurites in a voxel. For completeness, the commonly reported physical parameters (e.g. fractional anisotropy and mean diffusivity; Basser, 1995) that are often derived from diffusion data were also computed (Oeschger et al., 2021; see Appendix 1 and Supplementary files 1 and 2). However, these metrics lack biological specificity (Jensen and Helpern, 2010; Jones et al., 2013a) and, consequently, could not speak to our research questions.

To ensure an appropriate sample size and a wide range of autobiographical memory recall ability, we examined a large group of healthy young adults from the general population (n = 217; 109 female, 108 male; mean age of 29.0 years, SD = 5.60; age was restricted to between 20-41 years to limit the possible effects of aging).

All participants underwent the widely-used Autobiographical Interview (Levine et al., 2002), which provided a detailed metric characterising their autobiographical memory recall ability as well as a control measure. Diffusion and magnetisation transfer saturation MRI scans were obtained for each person to enable calculation of the MR g-ratio and the other measures. Our analyses were performed using weighted means from each of the three white matter tracts of interest rather than voxel-wise across the whole brain, reducing the potential for false positives (Marek et al., 2022).

Focusing on the fornix, uncinate fasciculus and parahippocampal cingulum bundle, and assuming that better autobiographical memory recall is associated with faster conduction velocity (e.g. Brancucci, 2012; Dicke and Roth, 2016; Reed and Jensen, 1992; Xi et al., 1999),

we predicted that variations in the MR g-ratio from some or all of these tracts would be associated with better autobiographical memory recall ability. We further sought to adjudicate between the scenarios outlined in Figure 1 to ascertain if better autobiographical memory recall was associated with an increase in myelin thickness. This would be reflected as a negative relationship between the MR g-ratio and autobiographical memory recall ability (Figure 1B, C and F – blue and red arrows). Alternatively, better autobiographical memory recall ability could be related to predominantly larger inner axon diameters of the fibres within the tracts. This would be observed in the form of a positive relationship between the MR g-ratio and autobiographical memory recall ability (Figure 1D and F – orange arrow).

Results

Autobiographical memory recall

We employed the widely-used Autobiographical Interview (Levine et al., 2002) to score autobiographical memory recall (see Materials and Methods for full details). The main measure of autobiographical memory recall ability was the mean number of "internal" details from the freely recalled autobiographical memories. Internal details are those that describe the specific past event in question, and are considered to reflect episodic information. Across the participants, the mean number of internal details provided per memory was 23.95 (*SD* = 7.25; range = 4.60–44.60).

As a control measure, the mean number of "external" details was also calculated from the autobiographical memory descriptions. External details pertain to semantic information about the past event, and other non-event information. Across the participants, the mean number of external details provided per memory was 5.35 (*SD* = 3.20; range = 0.8–17.40).

No relationships between autobiographical memory recall ability and fornix or uncinate fasciculus microstructure measures

We first investigated the fornix and uncinate fasciculus. None of the measures from either tract were associated with autobiographical memory recall ability. This was the case when using a corrected $p < 0.017$ (see Materials and Methods) or an uncorrected $p < 0.05$ threshold. Full details of these results are provided in Appendix 1 (Appendix 1–figures 1 and 2; Appendix 1–tables 1-4), with the source data available in Supplementary file 1.

Of note, and for completeness, we also performed exploratory analyses in six additional white matter tracts: the anterior thalamic radiation, the dorsal cingulum bundle, the forceps minor, the inferior longitudinal fasciculus, the inferior occipitofrontal fasciculus and the superior longitudinal fasciculus. However, as with the fornix and the uncinate fasciculus, none of the metrics from any of these tracts were associated with autobiographical memory recall ability, even when using an uncorrected $p < 0.05$ threshold (see Appendix 1– figures 3-8 and Appendix 1– tables 5-16 for full details).

As noted in the Introduction, traditional physical parameters (e.g. fractional anisotropy and mean diffusivity) were also extracted for all tracts but, given their lack of biological specificity (Jensen and Helpern, 2010; Jones et al., 2013a), these are reported in Appendix 1–tables 1-16.

The parahippocampal cingulum bundle

We found that variations in autobiographical memory recall ability were uniquely related to the microstructure of the parahippocampal cingulum bundle. This tract connects the hippocampus with the entorhinal, parahippocampal, retrosplenial and parietal cortices, and the anterior thalamus (Figure 3). Moreover, via other subdivisions of the cingulum bundle, it is indirectly connected with prefrontal regions including the medial prefrontal cortex. The

241 parahippocampal cingulum bundle is, therefore, well positioned for information transfer
242 between the key regions involved in autobiographical memory recall (Andrews-Hanna et al.,
243 2014; Maguire, 2001; Spreng et al., 2009; Svoboda et al., 2006).
244
245

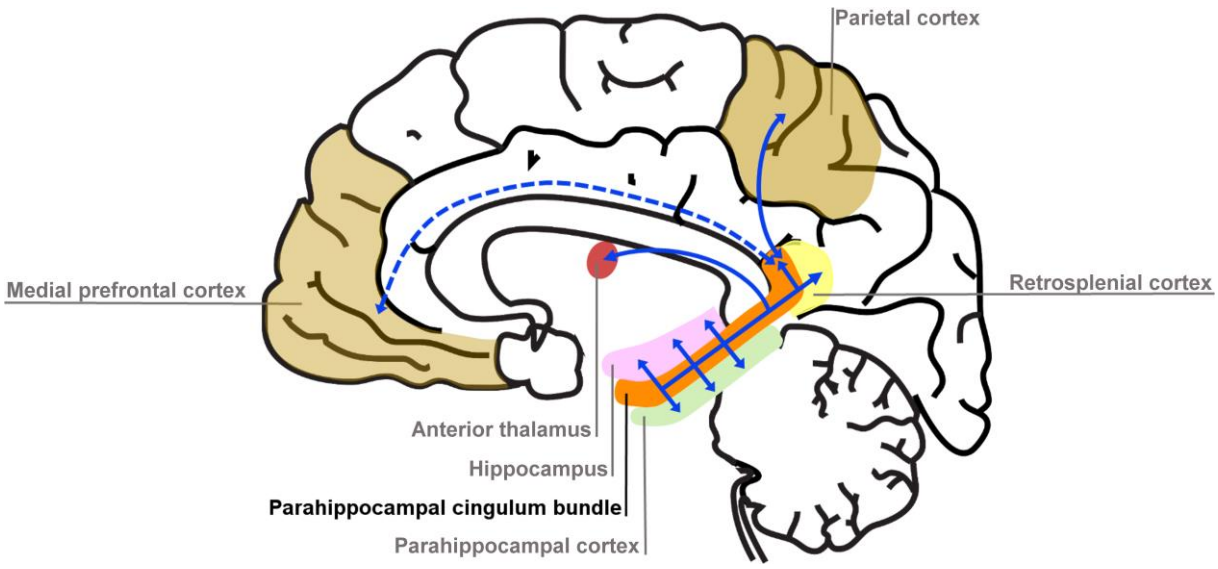

246

247 **Figure 3.** Simplified schematic of the location and main connections of the parahippocampal cingulum
248 bundle. The blue lines indicate direct connections, and the dashed blue line an indirect connection.
249

250 As with the other tracts (see Materials and Methods), the parahippocampal cingulum
251 bundle region of interest (ROI) was defined bilaterally using the Johns Hopkins probabilistic
252 white matter tractography atlas (Hua et al., 2008). To reduce partial volume effects, we used a
253 conservative minimum probability of 25%, and the tract ROI was refined for each participant
254 to ensure the mask was limited to each person's white matter. The mean number of voxels in
255 the parahippocampal cingulum bundle ROI was 129.11 (*SD* = 25.68), and the variance in
256 number of voxels across individuals was accounted for in our analyses. Table 1 shows the
257 summary statistics for the microstructure measures (see Appendix 1–tables 17 and 18,
258 Appendix 1–figures 9 and 10, and Supplementary file 2 for the traditional physical parameters,
259 e.g. fractional anisotropy, extracted from the parahippocampal cingulum bundle).

Table 1. Means and standard deviations for the microstructure measures from the parahippocampal cingulum bundle.

Microstructure Measure	Mean	Standard Deviation
MR g-ratio	0.647	0.043
Neurite dispersion (ODI)	0.189	0.038
Neurite density	0.480	0.051

Note. ODI = Orientation Dispersion Index

Greater MR g-ratio of the parahippocampal cingulum bundle was associated with better autobiographical memory recall

We first investigated whether the MR g-ratio of the parahippocampal cingulum bundle was associated with autobiographical memory recall ability, performing partial correlation analyses with age, gender, scanner and the number of voxels in the ROI included as covariates. A significant positive association was observed between the parahippocampal cingulum bundle MR g-ratio and the number of internal details (Figure 4A; $r(211) = 0.18$, $p = 0.008$, 95% CI = 0.05, 0.29). This relationship was specific to internal details, with no association evident for the external details control measure (Figure 4B; $r(211) = -0.09$, $p = 0.17$, 95% CI = -0.21, 0.019). Direct comparison of the correlations confirmed there was a significantly larger correlation between the MR g-ratio and internal details than for external details (Figure 4C; mean r difference = 0.28 (95% CI = 0.11, 0.45), $z = 3.21$, $p = 0.0013$). Therefore, when MR g-ratio values were higher in the parahippocampal cingulum bundle, suggesting the presence of fibres with larger inner axon diameters (see Figure 1D and 1F, orange arrow), better autobiographical memory recall was observed.

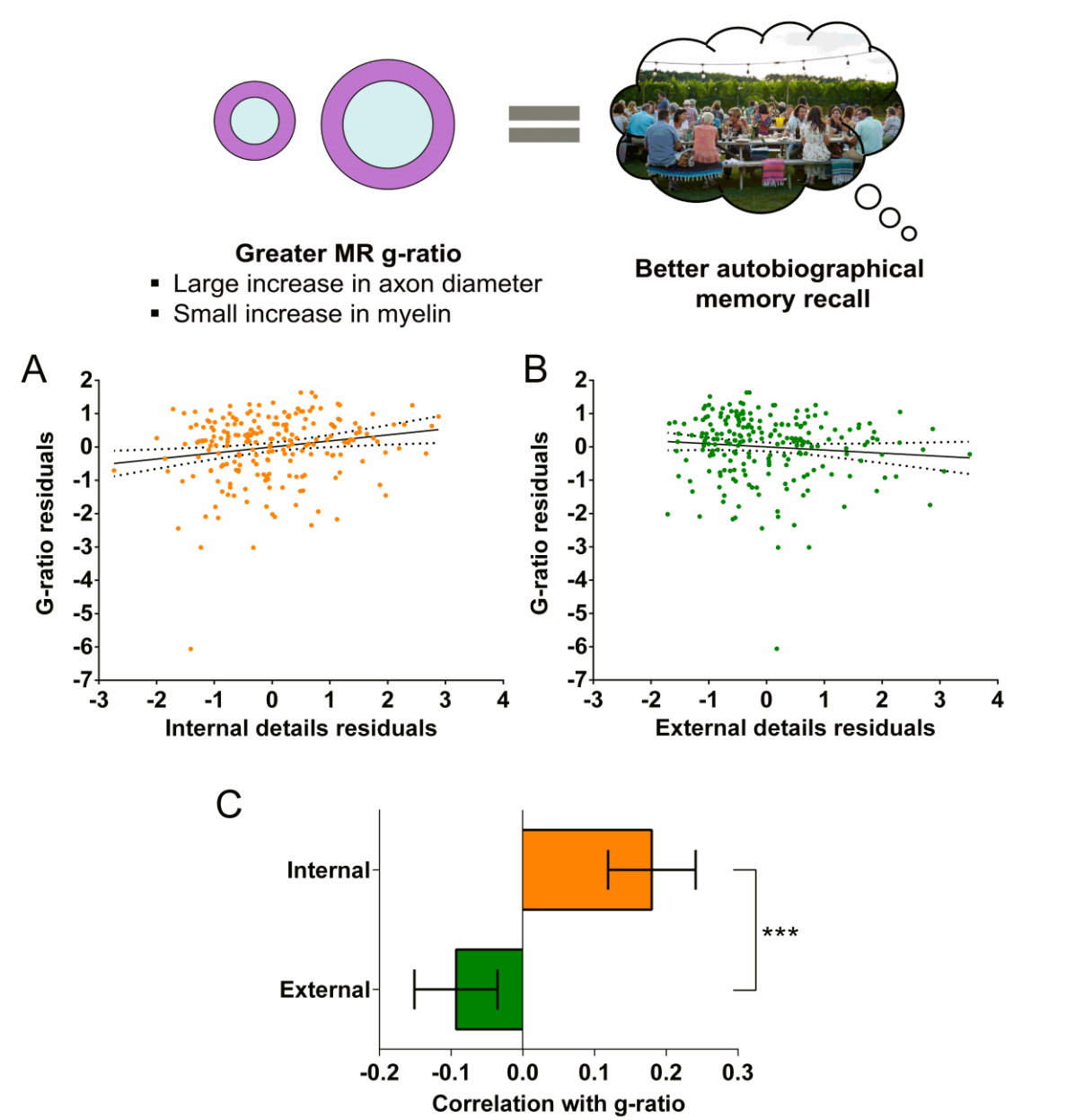

281

282 **Figure 4.** G-ratio and the parahippocampal cingulum bundle. The relationship between
283 parahippocampal cingulum bundle MR g-ratio and autobiographical memory recall ability (internal
284 details), and the control measure (external details) are shown. **(A)** There was a significant positive
285 correlation between g-ratio and internal details (dashed lines indicate the confidence intervals). **(B)**
286 There was no significant relationship between g-ratio and external details. **(C)** Bar chart showing the
287 partial correlation coefficients (with standard errors) between g-ratio and internal and external details.
288 There was a significant difference between the correlations when they were directly compared; ***$p <$
289 0.001. Data points for this figure are provided in Figure 4-source data 1.

Low neurite dispersion was related to better autobiographical memory recall

In addition to the MR g-ratio, we also examined the relationship between autobiographical memory recall ability and two complementary biological measures, the neurite orientation dispersion index and neurite density maps estimated using the NODDI biophysical model (Zhang et al., 2012). Partial correlations revealed a significant negative correlation between the neurite orientation dispersion index (a small orientation dispersion index value indicates low dispersion) and internal details (Figure 5A; $r(211) = -0.19$, $p = 0.005$, 95% CI = -0.32, -0.06). This was again specific to internal details with no significant relationship between the neurite orientation dispersion index and external details (Figure 5B; $r(211) = 0.07$, $p = 0.28$, 95% CI = -0.05, 0.20). Direct comparison of the correlations revealed a significantly larger correlation between the neurite orientation dispersion index and internal details than for external details (Figure 5C; mean r difference = 0.27 (95% CI = 0.44, 0.10), $z = 3.13$, $p = 0.0017$). Neurite density was not significantly related to either internal ($r(211) = 0.04$, $p = 0.60$, 95% CI = -0.09, 0.16), or external ($r(211) = 0.01$, $p = 0.93$, 95% CI = -0.12, 0.13) details. Therefore, in addition to a greater MR g-ratio, when neurites in the parahippocampal cingulum bundle were less dispersed and thus more coherently organised, this was associated with better autobiographical memory recall.

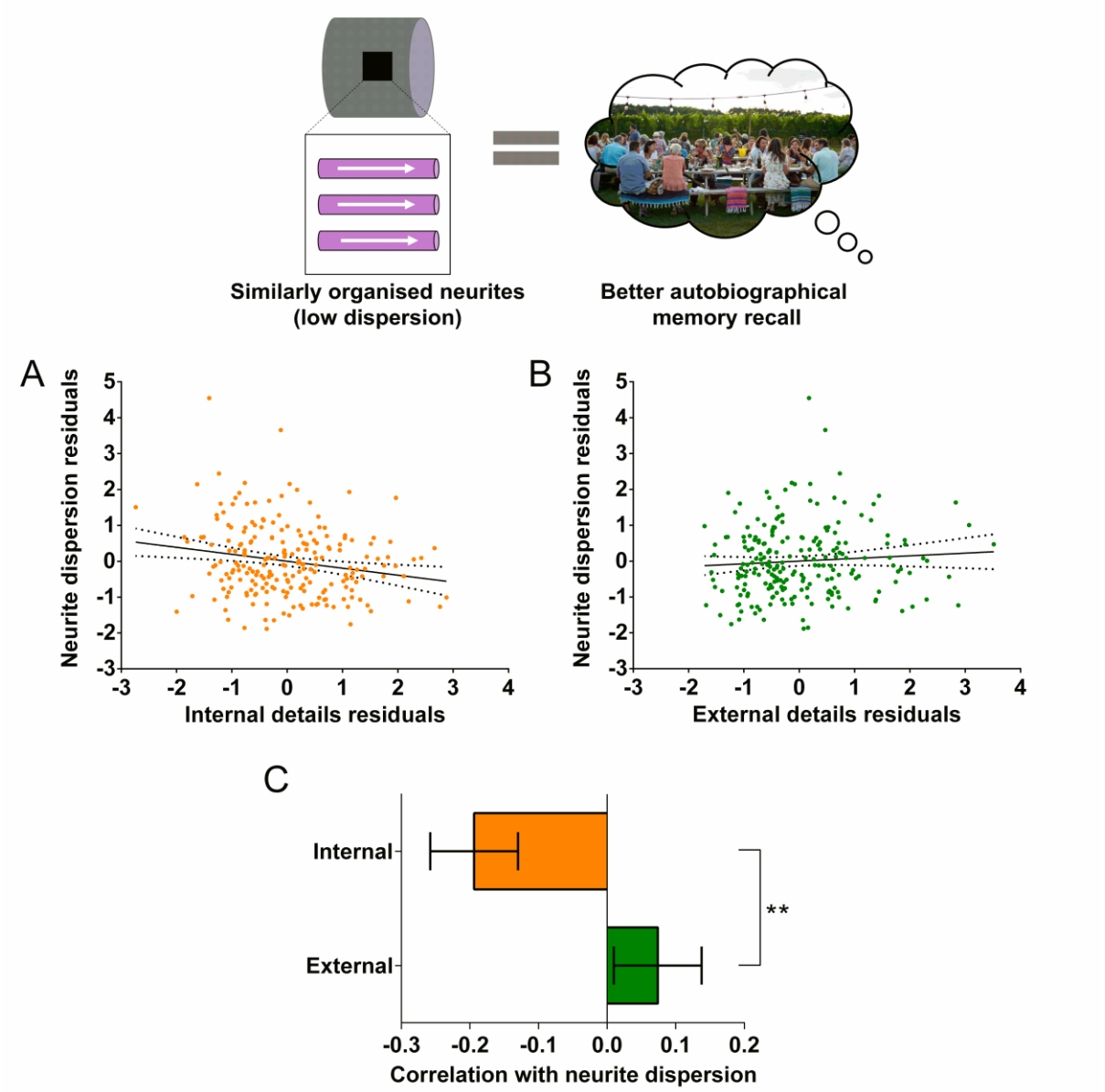

Figure 5. Neurite dispersion and the parahippocampal cingulum bundle. The relationship between parahippocampal cingulum bundle neurite dispersion (orientation dispersion index) and autobiographical memory recall ability (internal details), and the control measure (external details) are shown. **(A)** There was a significant negative correlation between neurite dispersion and internal details (dashed lines indicate the confidence intervals). **(B)** There was no significant relationship between neurite dispersion and external details. **(C)** Bar chart showing the partial correlation coefficients (with standard errors) between neurite dispersion and internal and external details. There was a significant difference between the correlations when they were directly compared; $^{**}p < 0.01$. Data points for this figure are provided in the Figure 5-source data 1.

Discussion

The conduction velocity of action potentials along axons is crucial for neural communication. Until recently it was not possible to examine metrics associated with axonal conduction velocity, such as the g-ratio, in vivo in the human brain, with this being largely the preserve of studies involving non-humans. However, by combining diffusion MRI with quantitative structural MRI scans optimised to assess myelination (Weiskopf et al., 2013), it is now possible to estimate the MR g-ratio in vivo in humans (Drakesmith et al., 2019; Mohammadi et al., 2015; Mohammadi and Callaghan, 2020; Stikov et al., 2015). Here, in the first application to human cognition, we found that variations in the MR g-ratio specifically in the parahippocampal cingulum bundle were associated with individual differences in autobiographical memory recall ability in a large sample of healthy adults. Moreover, we were able to identify two particular features in the parahippocampal cingulum bundle that might favour better memory recall, namely larger inner axon diameters, which are indicated by the increased MR g-ratio, and lower neurite dispersion, which suggests more coherently organised neurites. These results offer a new perspective on the neural instantiation of autobiographical memories, and in particular on drivers of individual differences in recall ability. This is especially welcome given the dearth of consistent findings linking hippocampal grey matter volume or microstructure with autobiographical memory recall ability in the healthy population (Clark et al., 2020; Clark et al., 2021a; LePort et al., 2012; Maguire et al., 2003; Van Petten, 2004).

Our use of a biophysical model of the MR signal enabled us to link our findings to different mechanistic processes in the underlying microstructure. We considered four scenarios involving axonal microstructure that could give rise to faster conduction velocities, which in turn might promote better memory recall. As shown in Figure 1, each of these axonal

346 microstructure changes has a different outcome in terms of the g-ratio. The positive relationship
347 we observed between the MR g-ratio and autobiographical memory recall ability suggests that
348 this effect was associated predominantly with greater inner axon diameter (Figure 1D and
349 Figure 1F, orange arrow). By contrast, had a negative correlation between the MR g-ratio and
350 autobiographical memory recall ability been identified, we could instead have inferred that an
351 increase in myelin was the relevant microstructural feature. Increases in myelination are often
352 held to be a prominent source of white matter alterations associated with changes in
353 behavioural and cognitive performance (Caeyenberghs et al., 2016; Kaller et al., 2017; Lakhani
354 et al., 2016; Waxman, 1980; Xin and Chan, 2020). By contrast, our results highlight the
355 potentially important role that the inner axon diameter could be playing in the recall of a critical
356 form of memory.

357 We also found that lower neurite dispersion, suggesting more coherent neurite
358 organisation, was related to better autobiographical memory recall ability. Our measure of
359 neurite dispersion was obtained using the NODDI biophysical model (Zhang et al., 2012),
360 which aims to isolate the organisation of the neurites in a voxel from the density of the neurites
361 in a voxel. While neurite dispersion was significantly related to autobiographical memory
362 recall, no relationship was observed with neurite density.

363 A larger inner axon diameter reduces resistance to action potential signals enabling
364 greater conduction velocities (Gasser and Grundfest, 1939; Hursh, 1939), and coherently
365 organised fibres may decrease the distance signals need to travel, further reducing
366 communication times (Salami et al., 2003; Steriade, 1995). This combination of features might
367 optimise a fibre bundle for faster communication which in turn may enhance autobiographical
368 memory recall.

369 These results were specific to one white matter tract, the parahippocampal cingulum
370 bundle (Bubb et al., 2018). MR g-ratio measures from no other tract, including the dorsal part

371 of the cingulum bundle, showed any association with autobiographical memory recall ability.
372 The parahippocampal cingulum bundle directly connects the hippocampus, parahippocampal,
373 retrosplenial and parietal cortices, the anterior thalamus and, through other subdivisions of the
374 cingulum bundle, the medial prefrontal cortex. These regions are typically engaged during
375 fMRI studies of autobiographical memory recall (Andrews-Hanna et al., 2014; Maguire, 2001;
376 Spreng et al., 2009; Svoboda et al., 2006), and damage to them is often associated with
377 autobiographical memory impairments (Berryhill et al., 2007; McCormick et al., 2018;
378 Scoville and Milner, 1957; Vann et al., 2009). The retrosplenial and parahippocampal cortices
379 are thought to provide visuospatial elements of autobiographical memories (Dalton and
380 Maguire, 2017; Epstein and Higgins, 2007; Mullally and Maguire, 2011; Vann et al., 2009),
381 while the medial prefrontal cortex may initiate autobiographical retrieval and support schema-
382 guided recall (Gilboa and Marlatte, 2017; McCormick et al., 2018; McCormick et al., 2020).
383 The parahippocampal cingulum bundle is, therefore, uniquely positioned as a transmission
384 highway enabling this information to reach the hippocampus, where memories can be
385 reconstructed (Bartlett, 1932; Hassabis and Maguire, 2007; Schacter et al., 2012). Larger inner
386 axon diameters and coherently organised neurites could facilitate rapid information flow along
387 the parahippocampal cingulum bundle leading to more memory elements being available
388 simultaneously, which in turn may result in increased detail and better integration of a memory
389 representation.

390 There have only been a small number of previous studies investigating white matter
391 tracts and individual differences in autobiographical memory recall ability in healthy people,
392 with some suggesting a relationship between the parahippocampal cingulum bundle and
393 autobiographical memory recall (Irish et al., 2014; Memel et al., 2020). However, interpretation
394 of those findings is difficult given the relatively small sample sizes, the older age of participants
395 in some of the studies, and the testing of mixed groups of healthy older people and patients

with dementia. No previous study has examined the MR g-ratio, instead they focussed on commonly reported physical parameters such as fractional anisotropy and mean diffusivity (Basser, 1995). However, these metrics lack biological specificity (Jensen and Helpern, 2010; Jones et al., 2013a) and, consequently, they cannot speak to questions concerning axonal conduction velocity. In a similar vein, we are not aware of any reports of bilateral lesions that selectively compromise or sever the parahippocampal cingulum bundle in humans. Given our findings, we would predict that such lesions would adversely affect the ability to recall autobiographical memories.

Despite its prime location and connectivity at the heart of the brain's autobiographical memory system, the dearth of studies in humans and the rarity of selective bilateral lesions to the parahippocampal cingulum bundle have perhaps obscured its importance when compared to other, more celebrated, memory-related white matter tracts. We also examined two such tracts, the fornix and the uncinate fasciculus, but in both cases no significant relationships between the MR g-ratio, neurite dispersion (or neurite density) and autobiographical memory recall ability were evident in our large cohort of young healthy adults. Both the fornix and parahippocampal cingulum bundle are vulnerable to partial volume effects (Concha et al., 2005). However, to mitigate this issue we took steps to ensure the data were extracted only from white matter voxels (see Materials and Methods). Diffusion data are also susceptible to distortions which can particularly affect the uncinate fasciculus. We addressed this challenge by using a new technique that improves distortion correction in this region (Clark et al., 2021b). The absence of fornix findings in our study could echo those relating to hippocampal volume (Clark et al., 2020; Clark et al., 2021a), whereby the structure is widely acknowledged to be involved in autobiographical memory recall, and damage impedes retrieval (Aggleton et al., 2000; D'Esposito et al., 1995; Gaffan and Gaffan, 1991; Tsivilis et al., 2008), but microstructural variations have limited impact within the healthy adult population. Regarding

421 the uncinate fasciculus, unilateral lesions do not seem to significantly impair performance on
422 laboratory-based memory tasks (Papagno et al., 2011) or the recall of premorbid
423 autobiographical memories (Levine et al., 2009). Bilateral uncinate fasciculus lesions are very
424 rare in humans, but might result in greater memory impairment. Alternatively, hippocampal-
425 prefrontal connections may be better served by other pathways, for example, via the fornix or
426 parts of the cingulum bundle.

427 Our findings were not only specific to the parahippocampal cingulum bundle, but also
428 to the internal details of autobiographical memories which reflect the episodicity of past
429 experiences. By contrast, our control measure of external details, which concerns non-episodic
430 information in the autobiographical memories, did not correlate with any white matter
431 microstructure metrics. In addition, age, gender, scanner and the number of voxels within an
432 ROI were included as covariates in all analyses, limiting the potential confounding effects of
433 these variables. Our analyses were also performed using weighted means from each of the three
434 white matter tracts of interest rather than voxel-wise across the whole brain, reducing the
435 potential for false positives (Marek et al., 2022).

436 While we examined the parahippocampal cingulum bundle as a unitary pathway, it
437 comprises both long and short association fibres with differing connectivity (Bubb et al., 2018).
438 Some fibres will form long range connections between, for example, the hippocampus and
439 retrosplenial cortex, whereas others will make shorter range connections between neighbouring
440 regions. The use of connectome MRI scanners is starting to make examination of short range
441 "u-fibres" possible in vivo in humans (Movahedian Attar et al., 2020; Shastin et al., pre print),
442 and future studies could seek to identify specific connections within the parahippocampal
443 cingulum bundle that relate to individual differences in autobiographical memory recall.

444 In conclusion, it is perhaps no surprise that speed may be of the essence when it comes
445 to neural communication, and this could influence individual differences in cognition.

Microstructure measures related to conduction velocity are now possible to derive in vivo in humans and have the potential to provide novel insights into how the brain processes and integrates information (Berman et al., 2019; Drakesmith et al., 2019), deepening our understanding of the information flow that underpins critical cognitive functions.

Materials and Methods

Participants

Two hundred and seventeen healthy people took part in the study, including 109 females and 108 males. The age range was restricted to 20-41 years old to limit the possible effects of aging (mean age = 29.0 years, *SD* = 5.60). Participants had English as their first language and reported no history of psychological, psychiatric or neurological conditions. People with hobbies or vocations known to be associated with the hippocampus (e.g. licenced London taxi drivers) were excluded. Participants were reimbursed £10 per hour for taking part which was paid at study completion. All participants gave written informed consent and the study was approved by the University College London Research Ethics Committee (project ID: 6743/001).

A sample size of 217 was determined during study design to be robust to employing different statistical approaches when answering multiple questions of interest. Specifically, the sample allowed for sufficient power to identify medium effect sizes when conducting correlation analyses at alpha levels of 0.01 and when comparing correlations at alpha levels of 0.05 (Cohen, 1992).

Procedure

Participants completed the study over multiple visits. Diffusion imaging and magnetisation transfer saturation scans were acquired on two separate days, and the Autobiographical Interview was conducted during a third visit. All participants completed all parts of the study.

The Autobiographical Interview

This widely-used test (Levine et al., 2002) was employed to measure autobiographical memory recall ability. Participants are asked to provide autobiographical memories from a specific time and place over four time periods – early childhood (up to age 11), teenage years (aged from 11-17), adulthood (from age 18 years to 12 months prior to the interview; two memories are requested) and the last year (a memory from the last 12 months); therefore, five memories in total are harvested. Recordings of the memory descriptions are transcribed for later scoring.

The main outcome measure of the Autobiographical Interview is the mean number of internal details included in the description of an event from across the five autobiographical memories. Internal details are those describing the event in question (i.e. episodic details) and include event, place, time and perceptual information, as well as thoughts and emotions relating to the event itself. We used the secondary outcome measure of the Autobiographical Interview, the mean number of external details included in the five autobiographical memories, as a control measure. External details include semantic information concerning the event, or other non-event information, and are not considered to reflect autobiographical memory recall ability.

Double scoring was performed on 20% of the data. Inter-class correlation coefficients, with a two-way random effects model looking for absolute agreement were calculated for both internal and external details. This was performed both for individual memories and as an average of all five memories across each participant. For internal details the coefficients were

0.94 and 0.97 respectively, and for external details they were 0.84 and 0.87 respectively. For reference, a score of 0.8 or above is considered excellent agreement beyond chance.

Diffusion MRI data acquisition

Three MRI scanners were used to collect the neuroimaging data. All scanners were Siemens Magnetom TIM Trio systems with 32 channel head coils and were located at the same neuroimaging centre, running the same software. The sequences were loaded identically onto the individual scanners. Participant set-up and positioning followed the same protocol for each scanner.

Diffusion-weighted images were collected using the multiband accelerated EPI pulse sequence developed by the Centre for Magnetic Resonance Research at the University of Minnesota (R012a-c, R013a on VB17, https://www.cmrr.umn.edu/multiband/; Feinberg et al., 2010; Xu et al., 2013). Acquisition parameters were: resolution = 1.7 mm isotropic; FOV = 220 mm × 220 mm × 138 mm; 60 directions with 6 interleaved b0 images, echo time (TE) = 112 ms, repetition time (TR) = 4.84 s, with a multiband acceleration factor of 3. The sequence was performed 4 times – twice with b-values of 1000 and twice with b-values of 2500. The first acquisition of each set of b-values was performed with phase-encoding in the anterior to posterior direction (blip-up), the second in the posterior to anterior direction (blip-down). The total acquisition time was 22 minutes.

Magnetisation transfer saturation data acquisition

The specific scanner used to collect a participant's diffusion-weighted images was also used to obtain their magnetisation transfer saturation map.

Whole brain structural maps of magnetisation transfer saturation, at an isotropic resolution of 800 μm, were derived from a multi-parameter mapping quantitative imaging

protocol (Callaghan et al., 2015; Callaghan et al., 2019; Weiskopf et al., 2013). This protocol consisted of the acquisition of three multi-echo gradient-echo acquisitions with either proton density, T1 or magnetisation transfer weighting. Each acquisition had a TR of 25 ms. Proton density weighting was achieved with an excitation flip angle of 6^0, which was increased to 21^0 to achieve T1 weighting. Magnetisation transfer weighting was achieved through the application of a Gaussian RF pulse 2 kHz off resonance with 4 ms duration and a nominal flip angle of 220^0. This acquisition had an excitation flip angle of 6^0. The field of view was 256 mm head-foot, 224 mm anterior-posterior, and 179 mm right-left. The multiple gradient echoes per contrast were acquired with alternating readout gradient polarity at eight equidistant echo times ranging from 2.34 to 18.44 ms in steps of 2.30 ms using a readout bandwidth of 488 Hz/pixel. Only six echoes were acquired for the magnetisation transfer weighted volume to facilitate the off-resonance pre-saturation pulse and subsequent spoiling gradient within the TR. To accelerate the data acquisition, partially parallel imaging using the GRAPPA algorithm was employed in each phase-encoded direction (anterior-posterior and right-left) with forty integrated reference lines and a speed up factor of two. Calibration data were also acquired at the outset of each session to correct for inhomogeneities in the RF transmit field (Lutti et al., 2010). The total acquisition time was 27 minutes.

Diffusion MRI pre-processing

The diffusion MRI data were processed using the ACID toolbox (www.diffusiontools.com) within SPM12 (www.fil.ion.ucl.ac.uk/spm). The weighted average consecutive HySCO pipeline described in Clark et al. (2021b) was followed, with the addition of multi-shell Position-Orientation Adaptive Smoothing (msPOAS; Becker et al., 2012) and Rician bias correction (André et al., 2014). In brief, the blip-up and blip-down data were first separately

corrected for motion and eddy current artefacts. Next, msPOAS was performed, followed by correction for susceptibility-related distortion artefacts using the HySCO2 module (Macdonald and Ruthotto, 2018; Ruthotto et al., 2012). Tensor fitting (Mohammadi et al., 2013) was then implemented separately on each of the distortion corrected blip-up and blip-down datasets to estimate FA maps. HySCO2 was then repeated using the distortion corrected and brain-masked FA maps as input instead of b0 images; the second HySCO2 field map being consecutively applied to the "pre-corrected" diffusion MRI data. Finally, Rician bias noise correction was employed on the distortion corrected data (André et al., 2014), before the data were combined using a weighted average to minimise information loss due to susceptibility distortion blurring induced by local spatial compression.

Magnetisation transfer saturation pre-processing

The magnetisation transfer saturation data were processed for each participant using the hMRI toolbox (Tabelow et al., 2019) within SPM12. The default toolbox configuration settings were used, with the exception that correction for imperfect spoiling was additionally enabled (Corbin and Callaghan, 2021). The output magnetisation transfer saturation map quantified the degree of saturation of the steady state signal induced by the application of the off-resonance pre-pulse, having accounted for spatially varying T_1 times and RF field inhomogeneity (Weiskopf et al., 2013).

Each participant's magnetisation transfer saturation map was segmented into white matter probability maps using the unified segmentation approach (Ashburner and Friston, 2005), but with no bias field correction (since the magnetisation transfer saturation map does not suffer from any bias field modulation) and using the tissue probability maps developed by Lorio et al. (2016).

568

569 **Diffusion model fitting**

570 The MR g-ratio was calculated according to Ellerbrock and Mohammadi (2018):

571

572 $$g_{MR} = \sqrt{1 - \frac{MVF_{MR}}{MVF_{MR}+AVF_{MR}}}$$

573

574 with MVF_{MR} being the myelin-volume fraction estimated from the magnetisation transfer
575 saturation map and AVF_{MR} being the axonal-volume fraction. The AVF_{MR} was estimated as
576 $AVF_{MR} = (1 - MVF_{MR})$ AWF according to Stikov et al. (2015), where AWF was obtained by
577 combining the intra-cellular fraction (ν_{icvf}) and isotropic fraction (ν_{iso}) maps from NODDI
578 (Zhang et al., 2012) as $AWF = (1 - \nu_{iso})\ \nu_{icvf}$. The magnetisation transfer saturation map
579 was obtained from the hMRI toolbox as described above. For calibration of the magnetisation
580 transfer saturation map to a myelin-volume fraction map ($MVF_{MR} = \alpha\ MT_{sat}$), we used the g-
581 ratio based calibration method as reported in Ellerbrock and Mohammadi (2018) and
582 Mohammadi and Callaghan (2020), with $\alpha = 0.1683$.

583 The NODDI biophysical model (Zhang et al., 2012) was also used to obtain maps of
584 the neurite orientation dispersion index and neurite density using the NODDI toolbox
585 (http://mig.cs.ucl.ac.uk/index.php?n=Tutorial.NODDImatlab).

586 Finally, for completeness, Axial-Symmetric DKI (Oeschger et al., 2021) was performed
587 on the pre-processed diffusion data using the ACID toolbox to generate maps of the more
588 commonly reported physical parameters of fractional anisotropy, mean diffusivity, mean
589 kurtosis, diffusivities parallel and diffusivities perpendicular.

590

591

Microstructure data extraction

Microstructure data extraction was performed in Montreal Neurological Institute (MNI) space. The diffusion and magnetisation transfer saturation maps were transformed from native to MNI space using the hMRI toolbox (Tabelow et al., 2019). This involved performing inter-subject registration using DARTEL (Ashburner, 2007) on the segmented magnetisation transfer saturation grey and white matter probability maps, with the resulting DARTEL template and deformations then used to normalize the diffusion and magnetisation transfer saturation maps to MNI space at 1.5 x 1.5 x 1.5mm.

Bilateral tract ROIs were defined using the Johns Hopkins probabilistic white matter tractography atlas (Hua et al., 2008). Our primary foci were the fornix, uncinate fasciculus and parahippocampal cingulum bundle. However, we also performed exploratory analyses on six other tracts - the anterior thalamic radiation, the dorsal cingulum bundle, forceps minor, inferior longitudinal fasciculus, inferior occipitofrontal fasciculus and superior longitudinal fasciculus. To reduce partial volume effects, for all tracts (with the exception of the fornix as the available fornix tract was not probabilistic) the minimum probability threshold was set to 25%. In addition, all of the tract ROIs were refined for each participant using their segmented magnetisation transfer saturation white matter probability map, with a minimum probability of 90% to limit the mask to white matter. This also served to remove any residual mis-alignment from the maps being transformed into MNI space, as no smoothing was performed to preserve the quantitative values. As this resulted in differing tract ROI sizes for each participant, the number of voxels in each tract for each participant was calculated. Mean values of the extracted microstructure metrics from the tract ROIs were determined using a weighted average, where voxels with higher white matter probabilities contributed more to the mean.

Statistical analyses

Analyses were performed in SPSS v27 unless otherwise stated. Data were summarised using means and standard deviations. There were no missing data, and no data needed to be removed from any analysis.

As we had different tract ROI sizes for each participant, we first assessed whether there were any relationships between the number of voxels in the tract ROIs and autobiographical memory recall ability. We performed partial correlations for each tract between the number of voxels in the tract ROI and the number of internal details on the Autobiographical Interview, with age, gender and scanner as covariates. No significant relationships were identified (all $r <$ 0.12, all $p > 0.1$). However, to ensure no residual effects were present, the number of voxels in a tract ROI was included as a covariate in the analyses.

In our main analyses, we first investigated the relationships between each microstructure measure and the number of internal details from the Autobiographical Interview using partial correlations, with bootstrapping performed 10,000 times to calculate confidence intervals. Four covariates were included in each partial correlation: age, gender, scanner and the number of voxels in a tract ROI. For these primary analyses, similar partial correlations were performed for the external details control measure. If an internal details correlation was significant, the internal and external details correlations were then directly compared in order to test for statistical difference using the technique described by Meng et al. (1992). This approach extends the Fisher z transformation, allowing for more accurate testing and comparison of two related correlations. The correlation comparison was performed using the R cocor package v1.1.3 (Diedenhofen and Musch, 2015).

As the microstructure measures were investigated across several tracts, we corrected for the repeated testing of the same measures across our three main tracts of interest (the fornix, the uncinate fasciculus and the parahippocampal cingulum bundle) using the Bonferroni

642 method; dividing alpha = 0.05 by 3. Consequently, associations with a two-sided *p*-value <
643 0.017 were considered significant. As the comparison of correlations was performed only when
644 a significant correlation was identified, a two-sided *p*-value < 0.05 was deemed significant.

645

646 ## Acknowledgments

647 Thanks to Anna Monk, Victoria Hotchin, Gloria Pizzamiglio and Alice Liefgreen for assistance
648 with data collection and scoring. Thanks also to Mohammad Ashtarayeh and Jan Malte
649 Oeschger for their support with implementing the diffusion model fitting and g-ratio
650 calculations.

651

652 ## Additional information

653 **Funding**

654 **Funder**: Wellcome

655 Grant reference numbers: 101759/Z/13/Z; 210567/Z/18/Z; 203147/Z/16/Z

656 **Author**: Eleanor A. Maguire

657

658 **Funder:** ERA-NET NEURON

659 Grant reference number: hMRI-ofSCI

660 **Author:** Martina Callaghan, Siawoosh Mohammadi

661

662 **Funder:** German Federal Ministry of Education and Research

663 Grant reference number: 01EW1711A and B

664 **Author:** Siawoosh Mohammadi

665

666 **Funder:** German Research Foundation

667 Grant reference numbers: MO 2397/5-1; MO 2397/4-1

668 **Author:** Siawoosh Mohammadi

669

670 **Funder:** Forschungszentrums Medizintechnik Hamburg

671 Grant reference numbers: 01fmthh2017

672 **Author:** Siawoosh Mohammadi

673

674 **Funder:** MRC and Spinal Research Charity

675 Grant reference number: MR/R000050/1

676 **Author:** Martina F. Callaghan

677

678 The funders had no role in study design, data collection and interpretation, or the decision to

679 submit the work for publication.

680

681 **Author contributions**

682 Ian A Clark: conceptualization, methodology, investigation, data scoring, formal analysis,

683 writing – original draft, writing - review & editing; Siawoosh Mohammadi: formal analysis,

684 writing - review & editing; Martina F Callaghan: Formal analysis, writing - review & editing;

Eleanor A. Maguire: conceptualization, methodology, funding acquisition, supervision, formal analysis, writing – original draft, writing - review & editing

Author ORCIDs

Ian A. Clark https://orcid.org/0000-0002-5678-2190

Siawoosh Mohammadi https://orcid.org/0000-0003-1311-9636

Martina F. Callaghan https://orcid.org/0000-0003-0374-1659

Eleanor A. Maguire https://orcid.org/0000-0002-9470-6324

Ethics

Human subjects: All participants gave written informed consent and the study was approved by the University College London Research Ethics Committee (project ID: 6743/001).

Additional files

- Appendix 1. Details of the simulation performed for Figure 1f. Investigation of the MR g-ratio, neurite orientation dispersion index, neurite density and physical parameters in the fornix and uncinate fasciculus - no significant relationships were identified. Exploratory analyses of the MR g-ratio, neurite orientation dispersion index, neurite density and physical parameters in other white matter tracts – no significant relationships were identified. Investigation of the physical parameters extracted from the parahippocampal cingulum bundle.
- Supplementary file 1. Microstructure and physical parameters data for the fornix and uncinate fasciculus.

- Supplementary file 2. Physical parameters data for the parahippocampal cingulum bundle and source data for Appendix 1-figures 9 and 10.
- Figure 4-source data 1
- Figure 5-source data 1
- Materials Design Analysis Reporting (MDAR) Form

Data availability

The data for every participant are provided in Figure 4-source data 1, Figure 5-source data 1, Supplementary file 1 and Supplementary file 2.

References

Aggleton JP, McMackin D, Carpenter K, Hornak J, Kapur N, Halpin S, Wiles CM, Kamel H, Brennan P, Carton S, Gaffan D (2000) **Differential cognitive effects of colloid cysts in the third ventricle that spare or compromise the fornix** *Brain* **123**:800-815. http://dx.doi.org/10.1093/brain/123.4.800

Aggleton JP, Wright NF, Rosene DL, Saunders RC (2015) **Complementary patterns of direct amygdala and hippocampal projections to the macaque prefrontal cortex** *Cerebral Cortex* **25**:4351-4373. http://dx.doi.org/10.1093/cercor/bhv019

André ED, Grinberg F, Farrher E, Maximov II, Shah NJ, Meyer C, Jaspar M, Muto V, Phillips C, Balteau E (2014) **Influence of noise correction on intra- and inter-subject variability of quantitative metrics in diffusion kurtosis imaging** *PloS One* **9**:e94531. http://dx.doi.org/10.1371/journal.pone.0094531

Andrews-Hanna JR, Saxe R, Yarkoni T (2014) **Contributions of episodic retrieval and mentalizing to autobiographical thought: Evidence from functional neuroimaging, resting-state connectivity, and fMRI meta-analyses** *NeuroImage* **91**:324-335. http://dx.doi.org/10.1016/j.neuroimage.2014.01.032

Arancibia-Cárcamo IL, Ford MC, Cossell L, Ishida K, Tohyama K, Attwell D (2017) **Node of Ranvier length as a potential regulator of myelinated axon conduction speed** *eLife* **6**:e23329. http://dx.doi.org/10.7554/eLife.23329

Ashburner J, Friston KJ (2005) **Unified segmentation** *NeuroImage* **26**:839-851. http://dx.doi.org/10.1016/j.neuroimage.2005.02.018

Ashburner J (2007) **A fast diffeomorphic image registration algorithm** *NeuroImage* **38**:95-113. http://dx.doi.org/10.1016/j.neuroimage.2007.07.007

Aston-Jones G, Rogers J, Shaver RD, Dinan TG, Moss DE (1985) **Age-impaired impulse flow from nucleus basalis to cortex** *Nature* **318**:462-464. http://dx.doi.org/10.1038/318462a0

744 Bartlett FC (1932) **Remembering: A study in experimental and social psychology**.
745 Cambridge University Press, Cambridge, England.
746 Basser PJ (1995) **Inferring microstructural features and the physiological state of tissues**
747 **from diffusion-weighted images** *NMR in Biomedicine* **8**:333-344.
748 http://dx.doi.org/10.1002/nbm.1940080707
749 Becker SMA, Tabelow K, Voss HU, Anwander A, Heidemann RM, Polzehl J (2012) **Position-**
750 **orientation adaptive smoothing of diffusion weighted magnetic resonance data**
751 **(POAS)** *Medical Image Analysis* **16**:1142-1155.
752 http://dx.doi.org/10.1016/j.media.2012.05.007
753 Berman S, West KL, Does MD, Yeatman JD, Mezer AA (2018) **Evaluating g-ratio weighted**
754 **changes in the corpus callosum as a function of age and sex** *NeuroImage* **182**:304-
755 313. http://dx.doi.org/10.1016/j.neuroimage.2017.06.076
756 Berman S, Filo S, Mezer AA (2019) **Modeling conduction delays in the corpus callosum**
757 **using MRI-measured g-ratio** *NeuroImage* **195**:128-139.
758 http://dx.doi.org/10.1016/j.neuroimage.2019.03.025
759 Berryhill ME, Phuong L, Picasso L, Cabeza R, Olson IR (2007) **Parietal lobe and episodic**
760 **memory: Bilateral damage causes impaired free recall of autobiographical**
761 **memory** *Journal of Neuroscience* **27**:14415.
762 http://dx.doi.org/10.1523/JNEUROSCI.4163-07.2007
763 Brancucci A (2012) **Neural correlates of cognitive ability** *Journal of Neuroscience Research*
764 **90**:1299-1309. https://doi.org/10.1002/jnr.23045
765 Bubb EJ, Metzler-Baddeley C, Aggleton JP (2018) **The cingulum bundle: Anatomy,**
766 **function, and dysfunction** *Neuroscience & Biobehavioral Reviews* **92**:104-127.
767 http://dx.doi.org/10.1016/j.neubiorev.2018.05.008
768 Bullock TH, Moore JK, Fields RD (1984) **Evolution of myelin sheaths: Both lamprey and**
769 **hagfish lack myelin** *Neuroscience Letters* **48**:145-148.
770 http://dx.doi.org/10.1016/0304-3940(84)90010-7
771 Caeyenberghs K, Metzler-Baddeley C, Foley S, Jones DK (2016) **Dynamics of the human**
772 **structural connectome underlying working memory training** *The Journal of*
773 *Neuroscience* **36**:4056. http://dx.doi.org/10.1523/JNEUROSCI.1973-15.2016
774 Callaghan MF, Josephs O, Herbst M, Zaitsev M, Todd N, Weiskopf N (2015) **An evaluation**
775 **of prospective motion correction (PMC) for high resolution quantitative MRI**
776 *Frontiers in Neuroscience* **9**. http://dx.doi.org/10.3389/fnins.2015.00097
777 Callaghan MF, Lutti A, Ashburner J, Balteau E, Corbin N, Draganski B, Helms G, Kherif F,
778 Leutritz T, Mohammadi S, Phillips C, Reimer E, Ruthotto L, Seif M, Tabelow K,
779 Ziegler G, Weiskopf N (2019) **Example dataset for the hMRI toolbox** *Data in Brief*
780 **25**:104132. http://dx.doi.org/10.1016/j.dib.2019.104132
781 Cercignani M, Giulietti G, Dowell NG, Gabel M, Broad R, Leigh PN, Harrison NA, Bozzali
782 M (2017) **Characterizing axonal myelination within the healthy population: a**
783 **tract-by-tract mapping of effects of age and gender on the fiber g-ratio**
784 *Neurobiology of Aging* **49**:109-118.
785 http://dx.doi.org/10.1016/j.neurobiolaging.2016.09.016
786 Chomiak T, Hu B (2009) **What is the optimal value of the g-ratio for myelinated fibers in**
787 **the rat CNS? A theoretical approach** *PloS One* **4**:e7754.
788 http://dx.doi.org/10.1371/journal.pone.0007754
789 Clark IA, Monk AM, Hotchin V, Pizzamiglio G, Liefgreen A, Callaghan MF, Maguire EA
790 (2020) **Does hippocampal volume explain performance differences on**
791 **hippocampal-dependent tasks?** *NeuroImage* **221**:117211.
792 http://dx.doi.org/10.1016/j.neuroimage.2020.117211

Clark IA, Callaghan MF, Weiskopf N, Maguire EA (2021a) **The relationship between hippocampal-dependent task performance and hippocampal grey matter myelination and iron content** *Brain and Neuroscience Advances* **5**:1-8. http://dx.doi.org/10.1177/23982128211011923

Clark IA, Callaghan MF, Weiskopf N, Maguire EA, Mohammadi S (2021b) **Reducing susceptibility distortion related image blurring in diffusion MRI EPI data** *Frontiers in Neuroscience* **15**:706473. https://dx.doi.org/10.3389/fnins.2021.706473

Cohen J (1992) **A power primer** *Psychological Bulletin* **112**:155-159. http://dx.doi.org/10.1037/0033-2909.112.1.155

Concha L, Gross DW, Beaulieu C (2005) **Diffusion tensor tractography of the limbic system** *American Journal of Neuroradiology* **26**:2267-2274.

Corbin N, Callaghan MF (2021) **Imperfect spoiling in variable flip angle T1 mapping at 7T: quantifying and minimising impact** *Magnetic Resonance in Medicine* **86**:693-708. http://dx.doi.org/10.1002/mrm.28720

Croxson PL, Johansen-Berg H, Behrens TEJ, Robson MD, Pinsk MA, Gross CG, Richter W, Richter MC, Kastner S, Rushworth MFS (2005) **Quantitative investigation of connections of the prefrontal cortex in the human and macaque using probabilistic diffusion tractography** *Journal of Neuroscience* **25**:8854-8866. http://dx.doi.org/10.1523/JNEUROSCI.1311-05.2005

D'Esposito M, Verfaellie M, Alexander MP, Katz DI (1995) **Amnesia following traumatic bilateral fornix transection** *Neurology* **45**:1546. http://dx.doi.org/10.1212/WNL.45.8.1546

Dalton MA, Maguire EA (2017) **The pre/parasubiculum: a hippocampal hub for scene-based cognition?** *Current Opinion in Behavioral Sciences* **17**:34-40. http://dx.doi.org/10.1016/j.cobeha.2017.06.001

Dicke U, Roth G (2016) **Neuronal factors determining high intelligence** *Philosophical Transactions of the Royal Society of London. Series B: Biological Sciences* **371**:20150180. http://dx.doi.org/10.1098/rstb.2015.0180

Diedenhofen B, Musch J (2015) **cocor: A comprehensive solution for the statistical comparison of correlations** *PloS One* **10**:e0121945. http://dx.doi.org/10.1371/journal.pone.0121945

Drakesmith M, Harms R, Rudrapatna SU, Parker GD, Evans CJ, Jones DK (2019) **Estimating axon conduction velocity in vivo from microstructural MRI** *NeuroImage* **203**:116186. http://dx.doi.org/10.1016/j.neuroimage.2019.116186

Ellerbrock I, Mohammadi S (2018) **Four in vivo g-ratio-weighted imaging methods: Comparability and repeatability at the group level** *Frontiers in Neuroscience* **39**:24-41. http://dx.doi.org/10.1002/hbm.23858

Epstein RA, Higgins JS (2007) **Differential parahippocampal and retrosplenial involvement in three types of visual scene recognition** *Cerebral Cortex* **17**:1680-1693. http://dx.doi.org/10.1093/cercor/bhl079

Feinberg DA, Moeller S, Smith SM, Auerbach E, Ramanna S, Glasser MF, Miller KL, Ugurbil K, Yacoub E (2010) **Multiplexed echo planar imaging for sub-second whole brain fMRI and fast diffusion imaging** *PloS One* **5**:e15710. http://dx.doi.org/10.1371/journal.pone.0015710

Gaffan D, Gaffan EA (1991) **Amnesia in man following transection of the fornix: A review** *Brain* **114**:2611-2618. http://dx.doi.org/10.1093/brain/114.6.2611

Gasser HS, Grundfest H (1939) **Axon diameters in relation to the spike dimensions and the conduction velocity in mammalian a fibers** *American Journal of Physiology* **127**:393-414. http://dx.doi.org/10.1152/ajplegacy.1939.127.2.393

Gilboa A, Marlatte H (2017) **Neurobiology of schemas and schema-mediated memory** *Trends in Cognitive Sciences* **21**:618-631. http://dx.doi.org/10.1016/j.tics.2017.04.013

Hassabis D, Maguire EA (2007) **Deconstructing episodic memory with construction** *Trends in Cognitive Sciences* **11**:299-306. http://dx.doi.org/10.1016/j.tics.2007.05.001

Hua K, Zhang J, Wakana S, Jiang H, Li X, Reich DS, Calabresi PA, Pekar JJ, van Zijl PCM, Mori S (2008) **Tract probability maps in stereotaxic spaces: Analyses of white matter anatomy and tract-specific quantification** *NeuroImage* **39**:336-347. http://dx.doi.org/10.1016/j.neuroimage.2007.07.053

Hursh JB (1939) **Conduction velocity and diameter of nerve fibers** *American Journal of Physiology* **127**:131-139. http://dx.doi.org/10.1152/ajplegacy.1939.127.1.131

Huxley AF, Stämpeli R (1949) **Evidence for saltatory conduction in peripheral myelinated nerve fibres** *Journal of Physiology* **108**:315-339. https://doi.org/10.1113/jphysiol.1949.sp004335

Irish M, Hornberger M, El Wahsh S, Lam BYK, Lah S, Miller L, Hsieh S, Hodges JR, Piguet O (2014) **Grey and white matter correlates of recent and remote autobiographical memory retrieval – Insights from the dementias** *PloS One* **9**:e113081. http://dx.doi.org/10.1371/journal.pone.0113081

Jensen JH, Helpern JA (2010) **MRI quantification of non-Gaussian water diffusion by kurtosis analysis** *NMR in Biomedicine* **23**:698-710. http://dx.doi.org/10.1002/nbm.1518

Jones DK, Knösche TR, Turner R (2013a) **White matter integrity, fiber count, and other fallacies: The do's and don'ts of diffusion MRI** *NeuroImage* **73**:239-254. http://dx.doi.org/10.1016/j.neuroimage.2012.06.081

Jones DK, Christiansen KF, Chapman RJ, Aggleton JP (2013b) **Distinct subdivisions of the cingulum bundle revealed by diffusion MRI fibre tracking: Implications for neuropsychological investigations** *Neuropsychologia* **51**:67-78. http://dx.doi.org/10.1016/j.neuropsychologia.2012.11.018

Jung W, Lee J, Shin H-G, Nam Y, Zhang H, Oh S-H, Lee J (2018) **Whole brain g-ratio mapping using myelin water imaging (MWI) and neurite orientation dispersion and density imaging (NODDI)** *NeuroImage* **182**:379-388. http://dx.doi.org/10.1016/j.neuroimage.2017.09.053

Kaller MS, Lazari A, Blanco-Duque C, Sampaio-Baptista C, Johansen-Berg H (2017) **Myelin plasticity and behaviour—connecting the dots** *Current Opinion in Neurobiology* **47**:86-92. http://dx.doi.org/10.1016/j.conb.2017.09.014

Lakhani B, Borich MR, Jackson JN, Wadden KP, Peters S, Villamayor A, MacKay AL, Vavasour IM, Rauscher A, Boyd LA (2016) **Motor skill acquisition promotes human brain myelin plasticity** *Neural Plasticity*:7526135. http://dx.doi.org/10.1155/2016/7526135

LePort AKR, Mattfeld AT, Dickinson-Anson H, Fallon JH, Stark CEL, Kruggel F, Cahill L, McGaugh JL (2012) **Behavioral and neuroanatomical investigation of Highly Superior Autobiographical Memory (HSAM)** *Neurobiology of Learning and Memory* **98**:78-92. http://dx.doi.org/10.1016/j.nlm.2012.05.002

Levine B, Svoboda E, Hay JF, Winocur G, Moscovitch M (2002) **Aging and autobiographical memory: Dissociating episodic from semantic retrieval** *Psychology and Aging* **17**:677-689. http://dx.doi.org/10.1037/0882-7974.17.4.677

Levine B, Svoboda E, Turner GR, Mandic M, Mackey A (2009) **Behavioral and functional neuroanatomical correlates of anterograde autobiographical memory in isolated retrograde amnesic patient M.L** *Neuropsychologia* **47**:2188-2196. http://doi.org/10.1016/j.neuropsychologia.2008.12.026

Lorio S, Fresard S, Adaszewski S, Kherif F, Chowdhury R, Frackowiak RS, Ashburner J, Helms G, Weiskopf N, Lutti A, Draganski B (2016) **New tissue priors for improved automated classification of subcortical brain structures on MRI** *NeuroImage* **130**:157-166. http://dx.doi.org/10.1016/j.neuroimage.2016.01.062

Lutti A, Hutton C, Finsterbusch J, Helms G, Weiskopf N (2010) **Optimization and validation of methods for mapping of the radiofrequency transmit field at 3T** *Magnetic Resonance in Medicine* **64**:229-238. http://dx.doi.org/doi:10.1002/mrm.22421

Macdonald J, Ruthotto L (2018) **Improved susceptibility artifact correction of echo-planar MRI using the alternating direction method of multipliers** *Journal of Mathematical Imaging and Vision* **60**:268-282. http://dx.doi.org/10.1007/s10851-017-0757-x

Maguire EA (2001) **Neuroimaging studies of autobiographical event memory** *Philosophical Transactions of the Royal Society of London. Series B: Biological Sciences* **356**:1441-1451. http://dx.doi.org/10.1098/rstb.2001.0944

Maguire EA, Valentine ER, Wilding JM, Kapur N (2003) **Routes to remembering: the brains behind superior memory** *Nature Neuroscience* **6**:90-95. http://dx.doi.org/10.1038/nn988

Marek S, Tervo-Clemmens B, Calabro FJ, Montez DF, Kay BP, Hatoum AS, Donohue MR, Foran W, Miller RL, Hendrickson TJ, Malone SM, Kandala S, Feczko E, Miranda-Dominguez O, Graham AM, Earl EA, Perrone AJ, Cordova M, Doyle O, Moore LA, Conan GM, Uriarte J, Snider K, Lynch BJ, Wilgenbusch JC, Pengo T, Tam A, Chen J, Newbold DJ, Zheng A, Seider NA, Van AN, Metoki A, Chauvin RJ, Laumann TO, Greene DJ, Petersen SE, Garavan H, Thompson WK, Nichols TE, Yeo BTT, Barch DM, Luna B, Fair DA, Dosenbach NUF (2022) **Reproducible brain-wide association studies require thousands of individuals** *Nature* **603**:654-660. http://dx.doi.org/10.1038/s41586-022-04492-9

McCormick C, Ciaramelli E, De Luca F, Maguire EA (2018) **Comparing and contrasting the cognitive effects of hippocampal and ventromedial prefrontal cortex damage: A review of human lesion studies** *Neuroscience* **274**:295-318. http://dx.doi.org/10.1016/j.neuroscience.2017.07.066

McCormick C, Barry DN, Jafarian A, Barnes GR, Maguire EA (2020) **vmPFC drives hippocampal processing during autobiographical memory recall regardless of remoteness** *Cerebral Cortex* **30**:5972-5987. http://dx.doi.org/10.1093/cercor/bhaa172

Memel M, Wank AA, Ryan L, Grilli MD (2020) **The relationship between episodic detail generation and anterotemporal, posteromedial, and hippocampal white matter tracts** *Cortex* **123**:124-140. http://dx.doi.org/10.1016/j.cortex.2019.10.010

Meng X-L, Rosenthal R, Rubin DB (1992) **Comparing correlated correlation coefficients** *Psychological Bulletin* **111**:172-175. http://dx.doi.org/10.1037/0033-2909.111.1.172

Miller EM (1994) **Intelligence and brain myelination: A hypothesis** *Personality and Individual Differences* **17**:803-832. http://dx.doi.org/10.1016/0191-8869(94)90049-3

Mohammadi S, Freund P, Feiweier T, Curt A, Weiskopf N (2013) **The impact of post-processing on spinal cord diffusion tensor imaging** *NeuroImage* **70**:377-385. http://dx.doi.org/10.1016/j.neuroimage.2012.12.058

Mohammadi S, Carey D, Dick F, Diedrichsen J, Sereno MI, Reisert M, Callaghan MF, Weiskopf N (2015) **Whole-brain in-vivo measurements of the axonal g-ratio in a group of 37 healthy volunteers** *Frontiers in Neuroscience* **9**. http://dx.doi.org/10.3389/fnins.2015.00441

Mohammadi S, Callaghan MF (2020) **Towards in vivo g-ratio mapping using MRI: unifying myelin and diffusion imaging** *Journal of Neuroscience Methods*:108990. https://dx.doi.org/10.1016/j.jneumeth.2020.108990

940 Movahedian Attar F, Kirilina E, Haenelt D, Pine KJ, Trampel R, Edwards LJ, Weiskopf N
941 (2020) **Mapping short association fibers in the early cortical visual processing**
942 **stream using in vivo diffusion tractography** *Cerebral Cortex* **30**:4496-4514.
943 http://dx.doi.org/10.1093/cercor/bhaa049
944 Mullally SL, Maguire EA (2011) **A new role for the parahippocampal cortex in**
945 **representing space** *The Journal of Neuroscience* **31**:7441-7449.
946 http://dx.doi.org/10.1523/JNEUROSCI.0267-11.2011
947 Nave K-A (2010) **Myelination and support of axonal integrity by glia** *Nature* **468**:244-252.
948 http://dx.doi.org/10.1038/nature09614
949 Oeschger J, Tabelow K, Mohammadi S (2021) **Reducing rician noise bias in axial-**
950 **symmetric diffusion kurtosis imaging and biophysical tissue models**, Proceedings
951 of the International Society for Magnetic Resonance in Medicine Scientific Meeting
952 and Exhibition, p. 3654.
953 Palombo DJ, Alain C, Söderlund H, Khuu W, Levine B (2015) **Severely deficient**
954 **autobiographical memory (SDAM) in healthy adults: A new mnemonic syndrome**
955 *Neuropsychologia* **72**:105-118.
956 http://dx.doi.org/10.1016/j.neuropsychologia.2015.04.012
957 Palombo DJ, Sheldon S, Levine B (2018) **Individual differences in autobiographical**
958 **memory** *Trends in Cognitive Sciences* **22**:583-597.
959 http://dx.doi.org/10.1016/j.tics.2018.04.007
960 Papagno C, Miracapillo C, Casarotti A, Romero Lauro LJ, Castellano A, Falini A, Casaceli G,
961 Fava E, Bello L (2011) **What is the role of the uncinate fasciculus? Surgical removal**
962 **and proper name retrieval** *Brain* **134**:405-414.
963 http://dx.doi.org/10.1093/brain/awq283
964 Peters A, Moss MB, Sethares C (2000) **Effects of aging on myelinated nerve fibers in**
965 **monkey primary visual cortex** *Journal of Comparative Neurology* **419**:364-376.
966 https://doi.org/10.1002/(SICI)1096-9861(20000410)419:3<364::AID-
967 CNE8>3.0.CO;2-R
968 Peters A, Sethares C (2002) **Aging and the myelinated fibers in prefrontal cortex and**
969 **corpus callosum of the monkey** *Journal of Comparative Neurology* **442**:277-291.
970 http://dx.doi.org/10.1002/cne.10099
971 Reed ET, Jensen AR (1993) **A somatosensory latency between the thalamus and cortex also**
972 **correlates with level of intelligence** *Intelligence* **17**:443-450.
973 http://dx.doi.org/10.1016/0160-2896(93)90011-S
974 Reed TE, Jensen AR (1992) **Conduction velocity in a brain nerve pathway of normal adults**
975 **correlates with intelligence level** *Intelligence* **16**:259-272.
976 http://dx.doi.org/10.1016/0160-2896(92)90009-G
977 Rushton WAH (1951) **A theory of the effects of fibre size in medullated nerve** *Journal of*
978 *Physiology* **115**:101-122. https://doi.org/10.1113/jphysiol.1951.sp004655
979 Ruthotto L, Kugel H, Olesch J, Fischer B, Modersitzki J, Burger M, Wolters CJPiM, Biology
980 (2012) **Diffeomorphic susceptibility artifact correction of diffusion-weighted**
981 **magnetic resonance images** *Physics in Medicine and Biology* **57**:5715.
982 http://dx.doi.org/10.1088/0031-9155/57/18/5715
983 Salami M, Itami C, Tsumoto T, Kimura F (2003) **Change of conduction velocity by regional**
984 **myelination yields constant latency irrespective of distance between thalamus and**
985 **cortex** *Proceedings of the National Academy of Sciences* **100**:6174.
986 http://dx.doi.org/10.1073/pnas.0937380100

Schacter DL, Addis DR, Hassabis D, Martin VC, Spreng RN, Szpunar KK (2012) **The future of memory: Remembering, imagining, and the brain** *Neuron* **76**:677-694. http://dx.doi.org/10.1016/j.neuron.2012.11.001

Schmidt H, Knösche TR (2019) **Action potential propagation and synchronisation in myelinated axons** *PLoS Computational Biology* **15**:e1007004. http://dx.doi.org/10.1371/journal.pcbi.1007004

Scoville WB, Milner B (1957) **Loss of recent memory after bilateral hippocampal lesions** *Journal of Neurology, Neurosurgery and Psychiatry* **20**:11-21. http://dx.doi.org/10.1136/jnnp.20.1.11

Shastin D, Genc S, Parker GD, Koller K, Tax CMW, Evans J, Hamandi K, Gray WP, Jones DK, Chamberland M (pre print) **Short association fibre tractography** *bioRxiv*:2021.2005.2007.443084. http://dx.doi.org/10.1101/2021.05.07.443084

Spreng RN, Mar RA, Kim ASN (2009) **The common neural basis of autobiographical memory, prospection, navigation, theory of mind, and the default mode: A quantitative meta-analysis** *Journal of Cognitive Neuroscience* **21**:489-510. http://dx.doi.org/10.1162/jocn.2008.21029

Steriade M (1995) **Two channels in the cerebellothalamocortical system** *Journal of Comparative Neurology* **354**:57-70. https://doi.org/10.1002/cne.903540106

Stikov N, Campbell JSW, Stroh T, Lavelée M, Frey S, Novek J, Nuara S, Ho M-K, Bedell BJ, Dougherty RF, Leppert IR, Boudreau M, Narayanan S, Duval T, Cohen-Adad J, Picard P-A, Gasecka A, Côté D, Pike GB (2015) **In vivo histology of the myelin g-ratio with magnetic resonance imaging** *NeuroImage* **118**:397-405. http://dx.doi.org/10.1016/j.neuroimage.2015.05.023

Svoboda E, McKinnon MC, Levine B (2006) **The functional neuroanatomy of autobiographical memory: A meta-analysis** *Neuropsychologia* **44**:2189-2208. http://doi.org/10.1016/j.neuropsychologia.2006.05.023

Tabelow K, Balteau E, Ashburner J, Callaghan MF, Draganski B, Helms G, Kherif F, Leutritz T, Lutti A, Phillips C, Reimer E, Ruthotto L, Seif M, Weiskopf N, Ziegler G, Mohammadi S (2019) **hMRI – A toolbox for quantitative MRI in neuroscience and clinical research** *NeuroImage* **194**:191-210. http://dx.doi.org/10.1016/j.neuroimage.2019.01.029

Tsivilis D, Vann SD, Denby C, Roberts N, Mayes AR, Montaldi D, Aggleton JP (2008) **A disproportionate role for the fornix and mammillary bodies in recall versus recognition memory** *Nature Neuroscience* **11**:834-842. http://dx.doi.org/10.1038/nn.2149

Tulving E (2002) **Episodic memory: From mind to brain** *Annual Review of Psychology* **53**:1-25. http://dx.doi.org/10.1146/annurev.psych.53.100901.135114

Van Petten C (2004) **Relationship between hippocampal volume and memory ability in healthy individuals across the lifespan: review and meta-analysis** *Neuropsychologia* **42**:1394-1413. http://dx.doi.org/10.1016/j.neuropsychologia.2004.04.006

Vann SD, Aggleton JP, Maguire EA (2009) **What does the retrosplenial cortex do?** *Nature Reviews: Neuroscience* **10**:792-802. http://dx.doi.org/10.1038/nrn2733

Von Der Heide RJ, Skipper LM, Klobusicky E, Olson IR (2013) **Dissecting the uncinate fasciculus: disorders, controversies and a hypothesis** *Brain* **136**:1692-1707. http://dx.doi.org/10.1093/brain/awt094

Waxman SG (1980) **Determinants of conduction velocity in myelinated nerve fibers** *Muscle & Nerve* **3**:141-150. https://doi.org/10.1002/mus.880030207

Weiskopf N, Suckling J, Williams G, Correia M, Inkster B, Tait R, Ooi C, Bullmore E, Lutti A (2013) **Quantitative multi-parameter mapping of R1, PD*, MT, and R2* at 3T: a multi-center validation** *Frontiers in Neuroscience* **7**. http://dx.doi.org/10.3389/fnins.2013.00095

West KL, Kelm ND, Carson RP, Does MD (2016) **A revised model for estimating g-ratio from MRI** *NeuroImage* **125**:1155-1158. http://dx.doi.org/10.1016/j.neuroimage.2015.08.017

West KL, Kelm ND, Carson RP, Alexander DC, Gochberg DF, Does MD (2018) **Experimental studies of g-ratio MRI in ex vivo mouse brain** *NeuroImage* **167**:366-371. http://dx.doi.org/10.1016/j.neuroimage.2017.11.064

Winocur G, Moscovitch M (2011) **Memory transformation and systems consolidation** *Journal of the International Neuropsychological Society* **17**:766-780. http://dx.doi.org/10.1017/s1355617711000683

Xi MC, Liu RH, Engelhardt JK, Morales FR, Chase MH (1999) **Changes in the axonal conduction velocity of pyramidal tract neurons in the aged cat** *Neuroscience* **92**:219-225. http://dx.doi.org/10.1016/S0306-4522(98)00754-4

Xin W, Chan JR (2020) **Myelin plasticity: sculpting circuits in learning and memory** *Nature Reviews Neuroscience* **21**:682-694. http://dx.doi.org/10.1038/s41583-020-00379-8

Xu J, Moeller S, Auerbach EJ, Strupp J, Smith SM, Feinberg DA, Yacoub E, Uğurbil K (2013) **Evaluation of slice accelerations using multiband echo planar imaging at 3T** *NeuroImage* **83**:991-1001. http://dx.doi.org/10.1016/j.neuroimage.2013.07.055

Yu F, Fan Q, Tian Q, Ngamsombat C, Machado N, Bireley JD, Russo AW, Nummenmaa A, Witzel T, Wald LL, Klawiter EC, Huang SY (2019) **Imaging g-ratio in multiple sclerosis using high-gradient diffusion MRI and macromolecular tissue volume** *American Journal of Neuroradiology* **40**:1871. http://dx.doi.org/10.3174/ajnr.A6283

Zhang H, Schneider T, Wheeler-Kingshott CA, Alexander DC (2012) **NODDI: Practical in vivo neurite orientation dispersion and density imaging of the human brain** *NeuroImage* **61**:1000-1016. http://dx.doi.org/10.1016/j.neuroimage.2012.03.072

Appendix 1

- **Details of the simulation performed for Figure 1F.**

- **Investigation of the MR g-ratio, neurite orientation dispersion index, neurite density and physical parameters in the fornix and uncinate fasciculus.**

- **Exploratory analyses of the MR g-ratio, neurite orientation dispersion index, neurite density and physical parameters in other white matter tracts.**

- **Investigation of the physical parameters extracted from the parahippocampal cingulum bundle.**

Details of the simulation performed for Figure 1F

In Figure 1F, inner axon diameter, myelin thickness and g-ratio are plotted together. The range of g-ratio values used in the simulation spanned two standard deviations about the mean MR g-ratio observed for the parahippocampal cingulum bundle in the current study (mean = 0.647, standard deviation = 0.043). The axon diameter was computed for this MR g-ratio range by re-arranging the equation presented in Berman et al. (2019) such that $\text{axon diameter} = \exp(\frac{\text{g-ratio}-0.506}{0.22})$. Fibre dimeter was then calculated as $\text{fibre diameter} = \frac{\text{axon diamter}}{\text{g-ratio}}$, enabling myelin thickness to be computed as $\text{myelin thickness} = \frac{\text{fibre diameter}-\text{axon diameter}}{2}$.

We note that discrepancies between reported microscopic parameters (i.e., g-ratio, modelled axon diameter, and myelin thickness) derived from in vivo and ex vivo histology may arise due to two reasons. (1) The in vivo MR g-ratio is computed from volume-fractions unlike the microscopic g-ratio measured with histology. (2) The heuristic equation by Berman et al. (2019) that is relating the in vivo MR g-ratio to axon diameter is rather capturing the tail of the axon radii distribution.

Investigation of the MR g-ratio, neurite orientation dispersion index, neurite density and physical parameters in the fornix and uncinate fasciculus

As can be observed in the tables below, there were no significant correlations between microstructural measures or physical parameters and autobiographical memory recall ability for either of the tracts when using the corrected ($p < 0.017$) threshold.

Fornix

The mean number of voxels in the region of interest (ROI) was 249.55 (SD = 23.09).

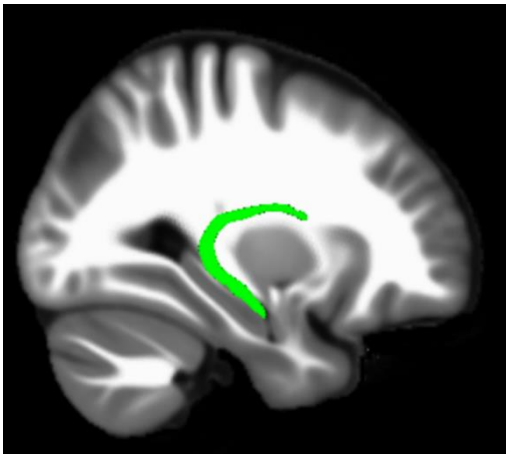

Appendix 1–figure 1. The location of the fornix.

Appendix 1–table 1. Means and standard deviations for the microstructure measures and physical parameters extracted from the fornix.

Measure	Mean	Standard Deviation
MR g-ratio	0.720	0.017
Neurite dispersion (ODI)	0.143	0.021
Neurite density	0.601	0.045
Fractional anisotropy	0.605	0.035
Mean diffusivity (10^{-3} mm^2/s)	0.901	0.036
Mean kurtosis	0.909	0.100
Diffusivities parallel (10^{-3} mm^2/s)	1.645	0.072
Diffusivities perpendicular (10^{-3} mm^2/s)	0.529	0.042

Note. ODI = Orientation Dispersion Index

Appendix 1–table 2. Partial correlations between the microstructure measures or physical parameters extracted from the fornix and memory recall ability (internal details).

Measure	r(211)	p	95% Confidence Interval	
			Lower	Upper
MR g-ratio	-0.04	0.53	-0.16	0.08
Neurite dispersion (ODI)	-0.03	0.62	-0.16	0.10
Neurite density	-0.03	0.69	-0.15	0.10
Fractional anisotropy	0.02	0.80	-0.12	0.15
Mean diffusivity	0.07	0.35	-0.08	0.21
Mean kurtosis	-0.03	0.66	-0.16	0.10
Diffusivities parallel	0.05	0.46	-0.09	0.19
Diffusivities perpendicular	0.02	0.74	-0.12	0.15

Note. ODI = Orientation Dispersion Index

Uncinate fasciculus

The mean number of voxels in the ROI was 191.98 (SD = 29.77).

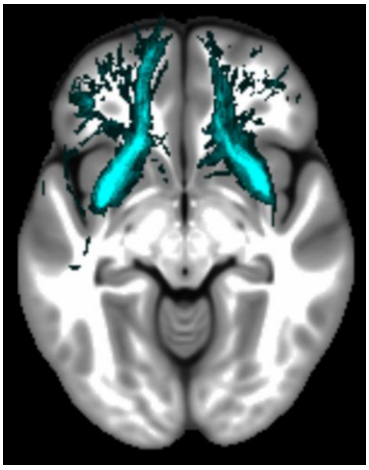

Appendix 1–figure 2. The location of the uncinate fasciculus.

Appendix 1–table 3. Means and standard deviations for the microstructure measures and physical parameters extracted from the uncinate fasciculus.

Measure	Mean	Standard Deviation
MR g-ratio	0.723	0.016
Neurite dispersion (ODI)	0.189	0.022
Neurite density	0.562	0.045
Fractional anisotropy	0.512	0.036
Mean diffusivity (10^{-3} mm^2/s)	0.877	0.304
Mean kurtosis	0.913	0.100
Diffusivities parallel (10^{-3} mm^2/s)	1.456	0.055
Diffusivities perpendicular (10^{-3} mm^2/s)	0.588	0.039

Note. ODI = Orientation Dispersion Index

Appendix 1–table 4. Partial correlations between the microstructure measures or physical parameters extracted from the uncinate fasciculus and memory recall ability (internal details).

Measure	r(211)	p	95% Confidence Interval	
			Lower	Upper
MR g-ratio	0.10	0.15	-0.03	0.22
Neurite dispersion (ODI)	-0.01	0.94	-0.14	0.13
Neurite density	0.01	0.89	-0.14	0.16
Fractional anisotropy	-0.01	0.94	-0.14	0.13
Mean diffusivity	-0.01	0.87	-0.14	0.13
Mean kurtosis	-0.01	0.91	-0.13	0.18
Diffusivities parallel	-0.01	0.87	-0.14	0.13
Diffusivities perpendicular	0.00	0.96	-0.15	0.14

Note. ODI = Orientation Dispersion Index

Exploratory analyses of the MR g-ratio, neurite orientation dispersion index, neurite density and physical parameters in other white matter tracts

As can be observed in the tables below, there were no significant correlations between microstructural measures or physical parameters and autobiographical memory recall ability for any of the tracts when using the corrected ($p < 0.017$) threshold.

Anterior thalamic radiation

The mean number of voxels in the ROI was 2090.21 (*SD* = 67.43).

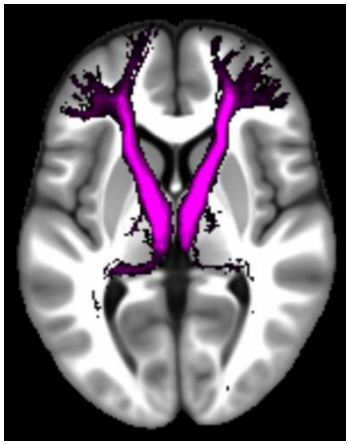

Appendix 1–figure 3. The location of the anterior thalamic radiation.

Appendix 1–table 5. Means and standard deviations for the microstructure measures and physical parameters extracted from the anterior thalamic radiation.

Measure	Mean	Standard Deviation
MR g-ratio	0.724	0.014
Neurite dispersion (ODI)	0.252	0.017
Neurite density	0.598	0.041
Fractional anisotropy	0.430	0.028
Mean diffusivity (10^{-3} mm^2/s)	0.861	0.029
Mean kurtosis	0.986	0.063
Diffusivities parallel (10^{-3} mm^2/s)	1.328	0.041
Diffusivities perpendicular (10^{-3} mm^2/s)	0.627	0.034

Note. ODI = Orientation Dispersion Index

Appendix 1–table 6. Partial correlations between the microstructure measures or physical parameters extracted from the anterior thalamic radiation and memory recall ability (internal details).

Measure	r(211)	p	95% Confidence Interval	
			Lower	Upper
MR g-ratio	0.05	0.47	-0.06	0.17
Neurite dispersion (ODI)	-0.05	0.46	-0.18	0.09
Neurite density	0.10	0.16	-0.04	0.23
Fractional anisotropy	0.08	0.26	-0.06	0.21
Mean diffusivity	0.03	0.67	-0.11	0.17
Mean kurtosis	0.07	0.28	-0.07	0.22
Diffusivities parallel	0.09	0.20	-0.04	0.21
Diffusivities perpendicular	-0.02	0.77	-0.16	0.12

Note. ODI = Orientation Dispersion Index

Dorsal cingulum bundle

The mean number of voxels in the ROI was 611.48 (*SD* = 25.29).

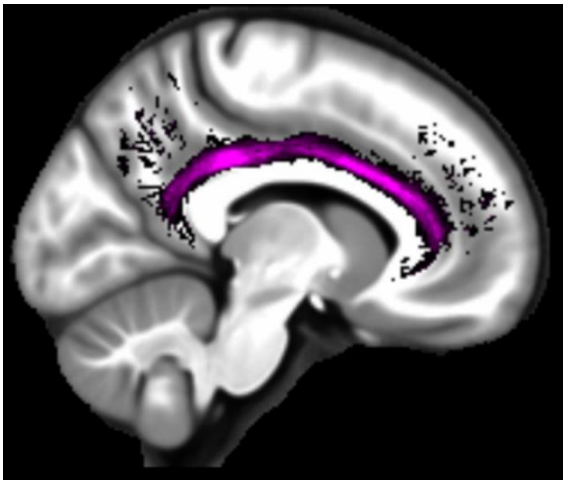

Appendix 1–figure 4. The location of the dorsal cingulum bundle.

Appendix 1–table 7. Means and standard deviations for the microstructure measures and physical parameters extracted from the dorsal cingulum bundle.

Measure	Mean	Standard Deviation
MR g-ratio	0.710	0.016
Neurite dispersion (ODI)	0.147	0.019
Neurite density	0.560	0.038
Fractional anisotropy	0.570	0.039
Mean diffusivity (10^{-3} mm^2/s)	0.862	0.026
Mean kurtosis	0.862	0.093
Diffusivities parallel (10^{-3} mm^2/s)	1.531	0.061
Diffusivities perpendicular (10^{-3} mm^2/s)	0.527	0.040

Note. ODI = Orientation Dispersion Index

Appendix 1–table 8. Partial correlations between the microstructure measures or physical parameters extracted from the dorsal cingulum bundle and memory recall ability (internal details).

Measure	r(211)	p	95% Confidence Interval Lower	Upper
MR g-ratio	0.09	0.22	-0.04	0.21
Neurite dispersion (ODI)	0.09	0.17	-0.05	0.23
Neurite density	0.09	0.17	-0.05	0.23
Fractional anisotropy	0.01	0.85	-0.13	0.16
Mean diffusivity	0.06	0.43	-0.08	0.19
Mean kurtosis	0.13	0.05	0.00	0.27
Diffusivities parallel	0.05	0.48	-0.08	0.18
Diffusivities perpendicular	0.01	0.91	-0.14	0.15

Note. ODI = Orientation Dispersion Index

Forceps minor

The mean number of voxels in the ROI was 4613.67 (*SD* = 78.02).

Appendix 1–figure 5. The location of the forceps minor.

Appendix 1–table 9. Means and standard deviations for the microstructure measures and physical parameters extracted from the forceps minor.

Measure	Mean	Standard Deviation
MR g-ratio	0.698	0.026
Neurite dispersion (ODI)	0.201	0.016
Neurite density	0.601	0.042
Fractional anisotropy	0.500	0.027
Mean diffusivity (10^{-3} mm^2/s)	0.881	0.031
Mean kurtosis	0.947	0.128
Diffusivities parallel (10^{-3} mm^2/s)	1.467	0.052
Diffusivities perpendicular (10^{-3} mm^2/s)	0.588	0.034

Note. ODI = Orientation Dispersion Index

Appendix 1–table 10. Partial correlations between the microstructure measures or physical parameters extracted from the forceps minor and memory recall ability (internal details).

Measure	r(211)	p	95% Confidence Interval	
			Lower	Upper
MR g-ratio	0.04	0.53	-0.07	0.18
Neurite dispersion (ODI)	-0.06	0.38	-0.21	0.07
Neurite density	0.09	0.19	-0.04	0.22
Fractional anisotropy	0.10	0.17	-0.03	0.23
Mean diffusivity	-0.04	0.56	-0.17	0.09
Mean kurtosis	0.00	0.97	-0.11	0.21
Diffusivities parallel	0.03	0.67	-0.09	0.18
Diffusivities perpendicular	-0.07	0.32	-0.19	0.05

Note. ODI = Orientation Dispersion Index

Inferior longitudinal fasciculus

The mean number of voxels in the ROI was 2844.03 (*SD* = 52.97).

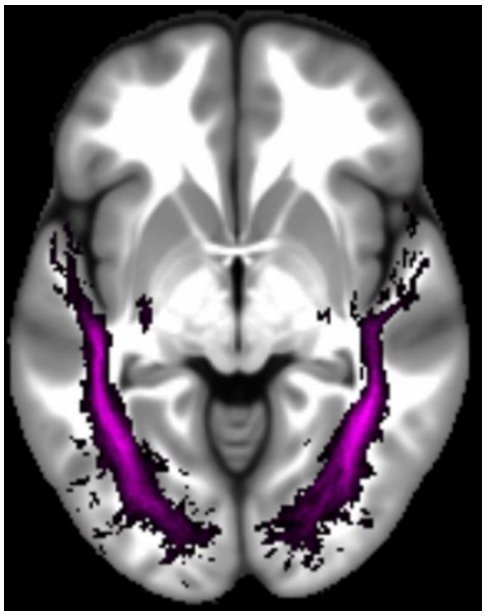

Appendix 1–figure 6. The location of the inferior longitudinal fasciculus.

Appendix 1–table 11. Means and standard deviations for the microstructure measures and physical parameters extracted from the inferior longitudinal fasciculus.

Measure	Mean	Standard Deviation
MR g-ratio	0.724	0.013
Neurite dispersion (ODI)	0.184	0.017
Neurite density	0.558	0.041
Fractional anisotropy	0.486	0.028
Mean diffusivity (10^{-3} mm^2/s)	0.902	0.029
Mean kurtosis	0.918	0.061
Diffusivities parallel (10^{-3} mm^2/s)	1.473	0.045
Diffusivities perpendicular (10^{-3} mm^2/s)	0.616	0.035

Note. ODI = Orientation Dispersion Index

Appendix 1–table 12. Partial correlations between the microstructure measures or physical parameters extracted from the inferior longitudinal fasciculus and memory recall ability (internal details).

Measure	r(211)	p	95% Confidence Interval	
			Lower	Upper
MR g-ratio	0.07	0.35	-0.06	0.19
Neurite dispersion (ODI)	-0.03	0.64	-0.17	0.10
Neurite density	0.07	0.35	-0.07	0.19
Fractional anisotropy	0.10	0.14	-0.04	0.23
Mean diffusivity	-0.01	0.87	-0.15	0.13
Mean kurtosis	0.10	0.16	-0.03	0.23
Diffusivities parallel	0.07	0.29	-0.07	0.21
Diffusivities perpendicular	-0.07	0.34	-0.19	0.07

Note. ODI = Orientation Dispersion Index

Inferior occipitofrontal fasciculus

The mean number of voxels in the ROI was 3344.31 (*SD* = 46.0).

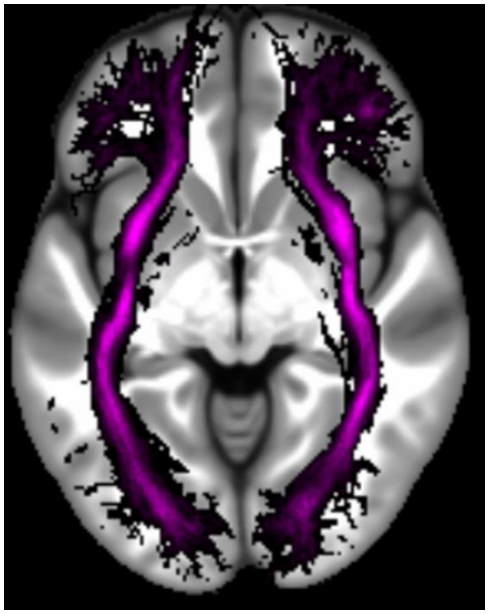

Appendix 1–figure 7. The location of the inferior occipitofrontal fasciculus.

Appendix 1–table 13. Means and standard deviations for the microstructure measures and physical parameters extracted from the inferior occipitofrontal fasciculus.

Measure	Mean	Standard Deviation
MR g-ratio	0.729	0.011
Neurite dispersion (ODI)	0.179	0.012
Neurite density	0.563	0.036
Fractional anisotropy	0.508	0.024
Mean diffusivity (10^{-3} mm^2/s)	0.889	0.026
Mean kurtosis	0.912	0.057
Diffusivities parallel (10^{-3} mm^2/s)	1.488	0.039
Diffusivities perpendicular (10^{-3} mm^2/s)	0.590	0.031

Note. ODI = Orientation Dispersion Index

Appendix 1–table 14. Partial correlations between the microstructure measures or physical parameters extracted from the inferior occipitofrontal fasciculus and memory recall ability (internal details).

Measure	r(211)	p	95% Confidence Interval	
			Lower	Upper
MR g-ratio	-0.01	0.93	-0.12	0.12
Neurite dispersion (ODI)	-0.01	0.89	-0.14	0.13
Neurite density	0.06	0.42	-0.07	0.18
Fractional anisotropy	0.06	0.38	-0.08	0.20
Mean diffusivity	0.00	0.99	-0.13	0.13
Mean kurtosis	0.07	0.31	-0.06	0.19
Diffusivities parallel	0.05	0.50	-0.09	0.18
Diffusivities perpendicular	-0.03	0.62	-0.17	0.10

Note. ODI = Orientation Dispersion Index

Superior longitudinal fasciculus

The mean number of voxels in the ROI was 4243.22 (*SD* = 39.80).

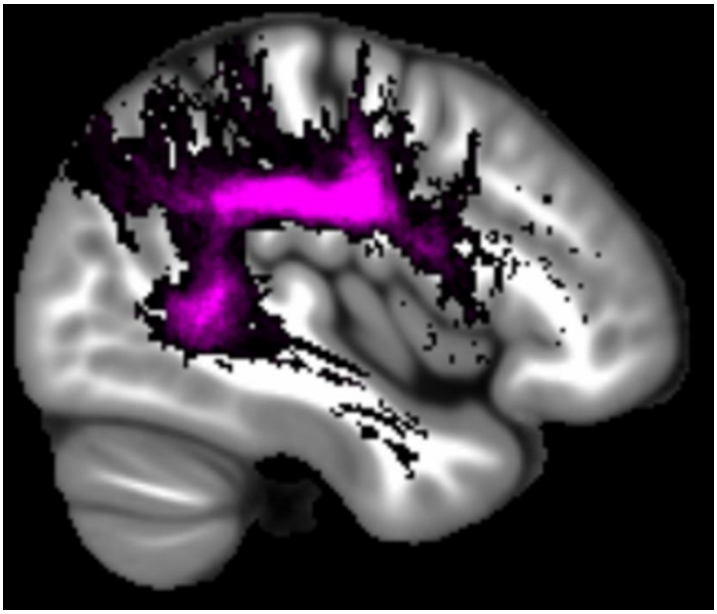

Appendix 1–figure 8. The location of the superior longitudinal fasciculus.

Appendix 1–table 15. Means and standard deviations for the microstructure measures and physical parameters extracted from the superior longitudinal fasciculus.

Measure	Mean	Standard Deviation
MR g-ratio	0.751	0.011
Neurite dispersion (ODI)	0.218	0.012
Neurite density	0.634	0.034
Fractional anisotropy	0.471	0.026
Mean diffusivity (10^{-3} mm^2/s)	0.825	0.025
Mean kurtosis	1.029	0.041
Diffusivities parallel (10^{-3} mm^2/s)	1.324	0.035
Diffusivities perpendicular (10^{-3} mm^2/s)	0.575	0.041

Note. ODI = Orientation Dispersion Index

Appendix 1–table 16. Partial correlations between microstructure measures or physical parameters extracted from the superior longitudinal fasciculus and memory recall ability (internal details).

Measure	r(211)	p	95% Confidence Interval	
			Lower	Upper
MR g-ratio	0.08	0.28	-0.05	0.20
Neurite dispersion (ODI)	-0.09	0.17	-0.23	0.05
Neurite density	0.12	0.09	-0.01	0.24
Fractional anisotropy	0.13	0.05	0.01	0.26
Mean diffusivity	-0.02	0.80	-0.14	0.11
Mean kurtosis	0.11	0.12	-0.03	0.24
Diffusivities parallel	0.12	0.09	-0.03	0.25
Diffusivities perpendicular	-0.08	0.23	-0.20	0.03

Note. ODI = Orientation Dispersion Index

Investigation of the physical parameters extracted from the parahippocampal cingulum bundle

As reported in the main text, significant correlations between a number of microstructural measures from the parahippocampal cingulum bundle and autobiographical memory recall ability were evident. This was also the case for several of the physical parameters – see Appendix 1–tables 17 and 18 and Appendix 1–figures 9 and 10 below.

Appendix 1–table 17. Means and standard deviations for the physical parameters extracted from the parahippocampal cingulum bundle.

Measure	Mean	Standard Deviation
Fractional anisotropy	0.466	0.053
Mean diffusivity (10^{-3} mm^2/s)	0.931	0.041
Mean kurtosis	0.779	0.122
Diffusivities parallel (10^{-3} mm^2/s)	1.479	0.071
Diffusivities perpendicular (10^{-3} mm^2/s)	0.656	0.057

Appendix 1–table 18. Partial correlations between the physical parameters extracted from the parahippocampal cingulum bundle and memory recall ability (internal details).

Measure	r(211)	p	95% Confidence Interval Lower	Upper
Fractional anisotropy	0.20	0.003*	0.07	0.32
Mean diffusivity	-0.02	0.72	-0.15	0.11
Mean kurtosis	0.08	0.23	-0.05	0.21
Diffusivities parallel	0.19	0.005*	0.06	0.32
Diffusivities perpendicular	0.15	0.03	-0.27	-0.02

* $p < 0.017$ (two-sided Bonferroni corrected threshold)

Specifically, partial correlation analyses, with age, gender, scanner and the number of voxels in the ROI included as covariates revealed a significant positive correlation between internal details and fractional anisotropy (FA) (Appendix 1–figure 9A; $r(211) = 0.20$, $p = 0.003$, 95%

CI = 0.07, 0.32). This relationship was specific to internal details, and was not evident for the external details control measure (Appendix 1–figure 9B; $r(211) = -0.06$, $p = 0.39$, 95% CI = -0.19, 0.07). Direct comparison of the two correlations confirmed a significant difference between them, showing that parahippocampal cingulum bundle FA was related to internal details to a greater extent than external details (Appendix 1–figure 9C; mean r difference = 0.26 (95% CI = 0.10, 0.44), $z = 3.08$, $p = 0.002$).

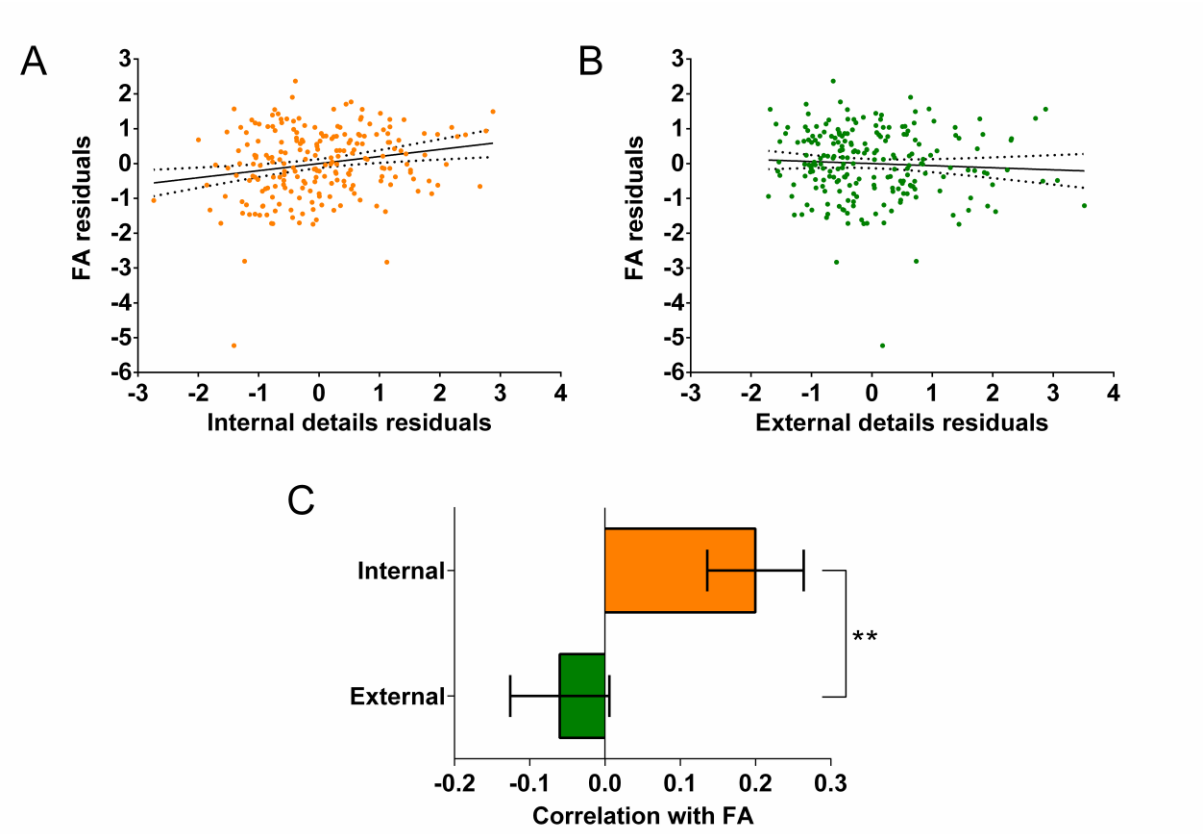

Appendix 1–figure 9. Fractional anisotropy (FA) and the parahippocampal cingulum bundle. The relationships between parahippocampal cingulum bundle FA and autobiographical memory recall ability (internal details), and the control measure (external details) are shown. **(A)** There was a significant positive correlation between FA and internal details (dashed lines indicate the confidence intervals). **(B)** There was no significant relationship between FA and external details. **(C)** Bar chart showing the partial correlation coefficients (with standard errors) between FA and internal and external details. There was a significant difference between the correlations when they were directly compared; $^{**}p < 0.01$. Data points for this figure are provided in Supplementary file 2.

In addition, a significant positive correlation between parallel diffusivity and the number of internal details was also apparent (Appendix 1–figure 10A; $r(211) = 0.19$, $p = 0.005$, 95% CI = 0.06, 0.32). As with FA, no significant relationship was observed between parallel diffusivity and external details (Appendix 1–figure 10B; $r(211) = -0.048$, $p = 0.49$, 95% CI = -0.19, 0.10). Direct comparison of the correlations confirmed that parallel diffusivity was related to internal details to a greater extent than external details (Appendix 1–figure 10C; mean r difference = 0.24 (95% CI = 0.07, 0.41), $z = 2.81$, $p = 0.0049$).

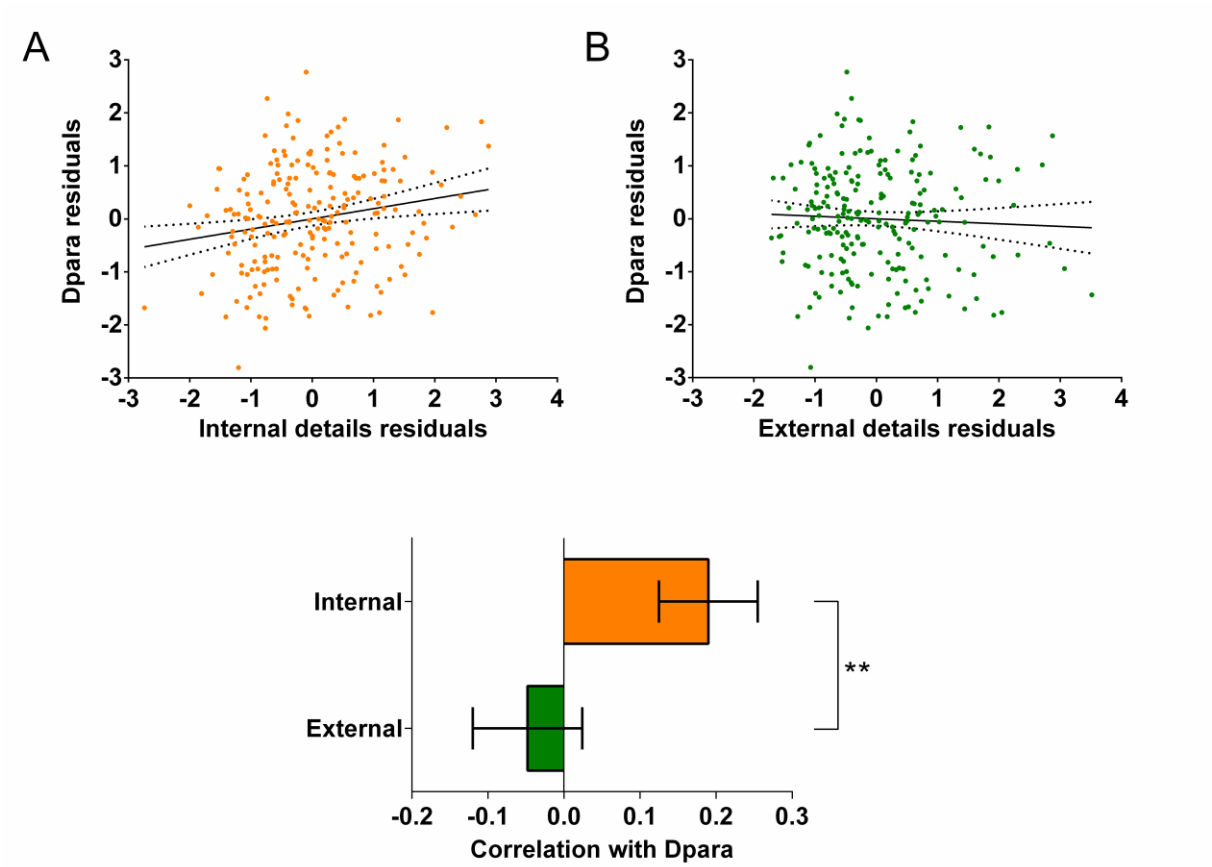

Appendix 1–figure 10. Dpara and the parahippocampal cingulum bundle. The relationships between parahippocampal cingulum bundle parallel diffusivity (Dpara) and autobiographical memory recall ability (internal details), and the control measure (external details) are shown. **(A)** There was a significant positive correlation between Dpara and internal details (dashed lines indicate the confidence intervals). **(B)** There was no significant relationship between Dpara and external details. **(C)** Bar chart showing the partial correlation coefficients (with standard errors) between Dpara and internal and external details. There was a significant difference between the correlations when they were directly compared; $^{**}p < 0.01$. Data points for this figure are provided in Supplementary file 2.

In contrast, no relationships were observed when examining the partial correlations between either internal or external details and MD (internal: $r(211) = -0.02$, $p = 0.72$, 95% CI = -0.15, 0.11; external: $r(211) = 0.01$, $p = 0.86$, 95% CI = -0.11, 0.14), the mean kurtosis (internal: $r(211) = 0.08$, $p = 0.23$, 95% CI = -0.05, 0.21; external: $r(211) = 0.03$, $p = 0.62$, 95% CI = -0.01, 0.16) or perpendicular diffusivity (internal: $r(211) = -0.15$, $p = 0.03$, 95% CI = -0.27, -0.02; external: $r(211) = 0.44$, $p = 0.52$, 95% CI = -0.08, 0.17), when using the corrected ($p < 0.017$) threshold. This suggests that none of these parameters were strongly associated with individual differences in autobiographical memory recall.